# Geomorphological impacts of an extreme flood in SE Spain

J. M. Hooke

Department of Geography and Planning, School of Environmental Sciences, University of Liverpool, Roxby Building, Liverpool, L69 7ZT, UK

Tel: 44 (0)151 794 2873

Email: janet.hooke@liverpool.ac.uk

**Abstract**

Long-term field studies in semiarid ephemeral streams are rare. These geomorphic data are essential for understanding the nature of the processes in order to develop modelling for risk assessments and management. An extreme flood event on 28 September 2012 affected the Murcia region of SE Spain, including long-tem monitoring sites on two fluvial systems in the Guadalentín basin, the Nogalte and Torrealvilla. Detailed morphological data were collected before and immediately after the event; and the amount of morphological change, erosion, and deposition have been related to peak flow conditions at the sites.

On the Nogalte channel, peak flow reached 2500 $m^3 s^{-1}$ at the downstream end of the catchment in less than one hour. The event had a recurrence interval of >50 years based on rainfall records and damage to old irrigation structures. The major effect in the braided, gravel channel of the Nogalte was net aggradation, with massive deposition in large flat bars. The measured changes in bankfull capacity were highly correlated with most hydraulic variables. Net changes in cut-and-fill in cross sections on the Nogalte were highly related to peak discharge and stream power but much less so to measures of hydraulic force (velocity, shear stress, unit stream power). Relationships of amount of erosion to hydraulic variables were much weaker than for amount of deposition, which was largely scaled to channel size and flow energy. Changes on the Torrealivlla were much less than on the Nogalte, and net erosion occurred at all sites. Sites on the Nogalte channel in schist exhibited higher deposition than those of the Torrealvilla sites on marl for the same hydraulic values.

Overall, less morphological change took place in the extreme event on the Nogalte than predicted from some published hydraulic relations, probably reflecting the high sediment supply and the hydrological characteristics of the event. The results demonstrate the high degree of adjustment of these channels to the occasional, high magnitude, flash flood events and that such events need to be allowed for in management. The detailed quantitative evidence produced by these long-term

34 monitoring sites provide valuable, rare data for modelling morphological response to flood events in
35 ephemeral channels.

36 *Key words:* flood; morphology; channel change; peak discharge; erosion; deposition; semiarid

## 1. Introduction

In semiarid areas, flow in channels is ephemeral, with occasional flash floods of varying magnitude. Large flash floods can result in fatalities and in major damage to infrastructure (Barredo, 2007; Lumbroso and Gaume, 2012) so it is of major importance to assess and quantify effects for management purposes, hazard mapping, and planning in order that the danger can be minimised and that the effects can be allowed for (Poesen and Hooke, 1997). Hazards not only may be caused by inundation and the direct effects of the flowing water but also by physical impacts of sediment movement, erosion, and deposition, and by the associated destruction. Geomorphologically, flood events are when the main changes take place in channels, and one of the major questions is the role of large floods and their relative contribution to sediment flux and to landscape changes. The trajectories of channels and the role of floods in contributing to altering those trajectories need to be understood and feedback effects of altered morphology incorporated in flood modelling (Hooke, 2015b). Data on effects of different flows are also needed to build predictive models of impacts of likely changes in flow regimes resulting from climate change and/or land use change (Hooke et al., 2005). Field data are required for model validation and to test principles and assumptions in models. Data are also needed to set the limits of uncertainty in any estimates and predictions. For all these reasons, documentation and measurement of the effects of major events is important, especially in ephemeral channels where such data are rare.

A major flash flood event occurred on 28 Sept 2012 in SE Spain, which resulted in 10 fatalities and much damage to infrastructure, including damage to bridges and roads, and much impact on agriculture (AON Benfield, 2012). It varied in magnitude and intensity across the region but is calculated from some hydrological parameters to be an extreme event on the European scale (Kirkby et al., 2013) and even on a world scale in terms of unit discharge (Thompson and Croke, 2013). This paper examines the morphological changes produced by the event in two channel systems by

63 analysing measurements at sites that have been continuously monitored for morphological change
64 since 1997 (Hooke, 2015b), specifically for the purpose of quantifying effects on morphology,
65 sediment, and vegetation of different size flows. Data capturing detailed measurements of impacts
66 of extreme events are rare, especially for such flash floods in semiarid environments, and difficult to
67 collect even when instrumentation is present (Coppus and Imeson, 2002). It is especially rare to
68 have before and after measurements of detailed topography and channel characteristics and at a
69 number of sites, as in this case. The amount and type of change is analysed in relation to hydraulics
70 of the flow event and the morphological characteristics of the sites. Nardi and Rinaldi (2015)
71 remarked that few examples of such relationships from flood events have been published.

72 Geomorphological impacts of case studies of high magnitude floods have been recorded, and forces
73 and dynamics of the events analysed recently (e.g., Fuller, 2008; Hauer and Habersack, 2009; Milan,
74 2012; Dean and Schmidt, 2013; Thompson and Croke, 2013) and in many (now classic) case studies
75 from the 1970s and 1980s (reviewed in Hooke, 2015b), but these are mainly in humid areas, on
76 perennially flowing streams. Many are in upland environments and involve effects on slope
77 instability and sediment influx as well as on channels. Studies of individual events in drylands and
78 the Mediterranean region include those of Harvey (1984) in SE Spain, on a channel of similar
79 characteristics to one studied here, and various studies elsewhere in Spain (e.g., Ortega and Garzón
80 Heydt, 2009), on the Magra River in Tuscany, Italy (Nardi and Rinaldi, 2015), in southern France
81 (Arnaud-Fasetta et al., 1993; Wainwright, 1996), in Israel (Schick and Lekach, 1987; Greenbaum and
82 Bergman, 2006; Grodek et al., 2012), and in SW USA (Huckleberry, 1994). Most of these studies do
83 not have prior morphological data. Hooke and Mant (2000) measured the effects of a flood in 1997
84 at the same sites as analysed here. Conesa-García (1995) previously assessed the effects of different
85 size events on one of these same channels. Some measurements of processes in flood events,
86 hydraulics of sediment transport and sediment dynamics, have been made at instrumented sites in
87 dryland areas, particularly in Israel (Laronne and Reid, 1993; Schick and Lekach, 1993; Reid et al.,
88 1995; Cohen et al., 2010) and at Walnut Gulch in Arizona (Powell et al., 2007; Nichols et al., 2008),

89 but also in Spain (Martin-Vide et al., 1999; Batalla et al., 2005); and measurement after events has
90 been used in modelling competence, capacity, and flux (Billi, 2008; Thompson and Croke, 2013).
91 Composite data on multiple extreme flood events were compiled by Baker and Costa (1987), Kochel
92 (1988), Newson (1989), Miller (1990), Magilligan (1992), and Costa and O'Connor (1995) in which
93 thresholds and extremes were identified and are commonly used as benchmarks for assessing
94 impacts. Prior morphological data of sufficient resolution are now becoming available through
95 LiDAR surveys and laser scanning, as exemplified in recent studies; for example, Hauer and
96 Habersack (2009) analysed changes in long reaches of channel where repeat terrestrial laser
97 scanner surveys were available, and Nardi and Rinaldi (2015) used LiDAR in combination with before-
98 and after-event aerial photographs. Various aspects of a large, infrequent flood event in
99 Queensland, Australia, have recently been investigated by Croke and her team (Croke et al., 2013;
100 Grove et al., 2013; Thompson and Croke, 2013; Thompson et al., 2013) using LiDAR.
101
102 A major theme in the geomorphological literature is that of magnitude-frequency of floods and the
103 relative morphological and sedimentological effects of different events. Various conceptual
104 frameworks are available for assessing the contribution in the longer term, notably through
105 sediment transport as a measure of amount of geomorphic work done (Wolman and Miller, 1960),
106 geomorphic effectiveness as a measure of change in landforms (Wolman and Gerson, 1978), and
107 effects of thresholds within the system that may produce sudden and large changes, or even
108 metamorphosis (Schumm, 1973, 1979). Flood impacts have been analysed in relation to various
109 measures of flood characteristics, including unit stream power (Magilligan, 1992), competence
110 (Jansen, 2006), and duration (Miller, 1990). LiDAR availability is extending the spatial scale of
111 analyses of flood impacts (e.g., Thompson and Croke, 2013). The importance of the physical setting
112 and spatial relations of reaches in determining flood impact is increasingly demonstrated by such
113 evidence and by comparison between morphologically contrasting reaches, particularly confined and
114 unconfined reaches (e.g., Cenderelli and Wohl, 2003). Documentation of impacts of extreme events

115 has shown that they vary widely with magnitude and other factors and that similar size floods can
116 have different effects at different times in the same location and that very different size floods can
117 have similar effects, depending on the state of the system and the flood characteristics (Hooke,
118 2015b).

119 Much data have been published on flood-generating conditions and identifying upper limits of
120 rainfall effects to feed into prediction and forecasting models. These are particularly important for
121 incorporating into assessments of impacts of future climate change and land use scenarios, both of
122 which are predicted to change markedly in the future in SE Spain (Herrera et al., 2010; Machado et
123 al., 2011). Most scenarios envisage an increase in desertification and therefore in runoff and soil
124 erosion. Much flood research focuses on the frequency and timing of flooding and on the conditions
125 generating the floods; a major EU project, HYDRATE (Gaume et al., 2009), has compiled much
126 hydrological and climatological data on extreme events. Extents of inundation and associated
127 hazards are relatively well documented, and much of the effort in the flood arena is now on
128 producing better predictive models of occurrence and impacts as a basis for flood risk management.
129 A major theme within this work is the documentation and modelling of connectivity down the river
130 system at a range of scales and between channel and floodplain (Thompson and Croke, 2013; Trigg
131 et al., 2013; Reaney et al., 2014). However, much more evidence and quantification of type,
132 amounts, and distributions of channel changes and physical impacts are needed to assess the
133 patterns, variability, and uncertainty for use in modelling and prediction. Flood modelling is still a
134 long way from incorporating feedback effects of morphological change (Wong et al., 2015).
135

136 The aims of this paper are (i) to quantify the physical impacts, amounts and scale of erosion and
137 deposition and their distribution in an extreme event on one channel, and in a moderately large
138 event on another channel, as measured on monitored reaches; (ii) to analyse the impacts in
139 relation to the event peak flow hydraulics and the channel morphology in order to understand the
140 controls and effects of conditions; and (iii) to compare these results to other published flood data.

## 2. Regional context and sites

The study area is located in the Guadalentín basin in SE Spain (Fig. 1). Monitored reaches were established in 1996/7 under the EU MEDALUS project (Hooke and Mant, 2015) specifically to test and validate a model of flood impacts and sequences of conditions that was being developed (Brookes et al., 2000; Hooke et al., 2005) because very little morphological change data existed for those or similar channels, nor data on sedimentological changes or interactions with vegetation and feedback on morphology, with which to validate the model. The region is semiarid with ~300 mm rainfall average. Three reaches, in the upper, middle, and lower parts of each of three channel systems were set up in 1996; these are (from south to north) the Nogalte, Torrealvilla (Fig. 1), and the Salada, near Murcia (Hooke, 2007). These were selected because of differing bedrock (Nogalte schist, others marl) and to provide a range of morphology, sediment, and vegetation conditions (Table 1). The sites were located in different parts of the catchment also to increase the likelihood of measuring flows because many flows are highly localised and do not persist down the channel (Hooke and Mant, 2002b). The sites are all within the upland area, mostly in well-defined valleys (Fig. 2). The area is mainly rural with dryland agriculture, dominated now by almond and olive cultivation. Irrigated agriculture occurs in parts of the area. Much of the slopes are afforested as part of the policy of flood control, and many check dams have been built along the water courses, particularly in the headwaters. Some land is still seminatural and abandoned from an earlier phase of agricultural decline; and the remains of old infrastructure from irrigation systems, mostly unused now, still survive in many places (Hooke and Mant, 2002a). The last two decades have seen agricultural intensification and rehabilitation and also much urban expansion and increase in modern infrastructure.

The focus in this paper is on the Nogalte in particular, affected by a large magnitude event, and on the Torrealvilla, where the event was moderate. The pre-flood state of each of the sites in the

Nogalte and Torrealvilla can be seen in Figure 2, and in comparison with the post-flood state. The characteristics of each site are provided in Table 1. The Nogalte is a schist catchment and the channel is composed of very loose, friable gravel with limited, very coarse material. Some narrow, confined bend reaches occur; but much of the course, including the monitored reaches, is braided, comprising low relief channels, with the full, active channel width occupying much of the valley floor. A main, primary, or inner (low flow) channel (Hooke and Mant, 2002b) is present but multiple minor channels flow across the braid bars (Fig. 2A). The extensive gravel bars are mostly vegetated by *Retama spp.* bushes. The Torrealvilla is in marl bedrock with overlying extensive gravel terraces on the upper slopes. The marl is highly erodible, and sediment load ranges from cobbles to silt-clay. The channels are mostly confined in narrow valleys and are predominantly single, wandering channels (Fig. 2B). Some check dams are present in the main stem and in tributary headwaters, including some that were destroyed in the 1997 event (Hooke and Mant, 2002a) and have since been rebuilt.

*2.1. September 2012 event*

The flood event took place on 28 September 2012 and affected much of SE Spain (http://www.bbc.co.uk/news/world-europe-19767627). The most severely affected parts were in southern Murcia and northeast Andalucía. Within the Guadalentín basin, the most intense and highest rainfalls were in the south of the basin and resulted in five fatalities in the Nogalte itself as well as severe damage to roads, bridges, bank protection, and irrigational and agricultural structures. The hydrological characteristics of the event have been analysed by Kirkby et al. (2013) and by the CHS (Confederación Hidrográfica del Segura) (https://www.chsegura.es/chs/informaciongeneral/comunicacion/noticias/noticia_1024.html). Intense rainfall took place after a very hot, dry summer. Total rainfall was measured as 161 mm in the storm over a few hours at Puerto Lumbreras at the downstream end of the Nogalte (Fig. 1) and as 73.4 mm in Lorca , downstream of the Torrealvilla (Fig. 1), but could have approached 250 mm in

191 the upper Nogalte (Kirkby et al., 2013; Smith et al., 2014) and exceeded 313 mm in Almeria province
192 (Riesco Martin et al., 2014). Rainfall averaged 80 mm from gauge records in the area around the
193 upper Torrealvilla (CHS data). Total rainfall has been estimated on the order of a 200-year
194 recurrence interval (RI) for Puerto Lumbreras (Kirkby et al., 2013) and, extrapolating from existing
195 records, to be of 100-year RI in the Torrealvilla (Bracken et al., 2008). Peak rainfall intensities
196 reached 81 mm $h^{-1}$ for an hour at Puerto Lumbreras. The stream gauge record there indicates a rise
197 to peak of 2500 $m^3 s^{-1}$ in 1 hour (Fig. 3A); on the Guadalentín at Lorca, to which the Torrealvilla is a
198 tributary, the rise was 538 $m^3 s^{-1}$ in 3 hours. Total durations to negligible flow were 4 and 21 hours
199 for the Nogalte and Guadalentín, respectively. Peak discharges have been calculated from flood
200 marks surveyed at cross sections down the main Nogalte channel soon after the event (Fig. 3B).
201 Specific discharges on the Nogalte reached values at, or even exceeding, the envelope for extreme
202 flash floods in Europe compiled in the EU HYDRATE project (Kirkby et al., 2013; Gaume et al., 2009),
203 exceeding 100 $m^3 s^{-1} km^{-2}$ in upper parts of the catchment. The CHS reported that rain gauges
204 showed maximum daily intensity of 179 $l/m^2$ (179 mm), with an intensity of 17 $l/m^2$ (17 mm) in five
205 minutes. The high precipitation in the upper Guadalentín was prevented from producing a more
206 intense flood downstream at Lorca by the dams of Valdinferno and Puentes, built mainly for flood
207 prevention
208 (https://www.chsegura.es/chs/informaciongeneral/comunicacion/noticias/noticia_1024.html).
209 Flood marks indicate that flow was continuous down the Nogalte and Torrealvilla channels and high
210 connectivity of runoff.

211 The Nogalte catchment includes the town of Puerto Lumbreras at the downstream end (Fig. 1). This
212 is the location of a previous catastrophic flood in October 1973 when a market was being held in the
213 river channel (Mairota et al., 1998). That flood resulted in 86 casualties and had much influence on
214 subsequent flood management policy. The peak flow of the 2012 event exceeded the 1973 event
215 according to the gauged data at Puerto Lumbreras: 2500 $m^3 s^{-1}$ in 2012 compared with 1161 $m^3 s^{-1}$ in
216 1973 (Navarro Hervás, 1991) but 2000 $m^3 s^{-1}$ according to Conesa García (1995). The flow is of at

217 least 50-year RI and possibly greater judging by the rainfall and the damage to old structures. Much
218 less damage occurred within the town this time because of raised flood walls and bed structures and
219 better flood warning. The event covered the whole catchment in 2012 rather than just the
220 headwaters as in 1973. In the Torrealvilla, the 2012 event was comparable in size with the
221 September 1997 event (Bull et al., 1999; Hooke and Mant, 2000) at the upstream site (Oliva) on the
222 main stem but was much higher on some tributaries, including the Prado (Aqueduct site) and at the
223 downstream end (Pintor site, near previous Serrata site) (Hooke and Mant, 2000; Smith et al., 2014;
224 Fig. 1). The 1997 rainfall was previously estimated as having a 7-year RI (Bull et al., 1999).

225

226 **3. Methods**

227 The flood event of 28 September 2012 affected sites in the Nogalte and Torrealvilla channels that
228 had been established in 1996/7 in order to measure the effects of a range of flows. From upstream
229 to downstream these are named Nog 1, Nog 2, and Nog Mon on the Nogalte, and on the Torrealvilla,
230 Oliva, Aqueduct (Aqued), and Pintor (Fig. 1). These reaches are 100-200 m in length and were set up
231 to measure changes in morphology, sediment, and vegetation, providing a representative range of
232 the characteristics (Table 1). Details of the methods are provided in Hooke (2007). At least annual
233 surveys have been carried out and more frequent measurements in certain periods and after major
234 events (Hooke, 2015a). All the sites were surveyed in November 2012 immediately following the
235 flood, and additional measurements were made in January 2013. Morphological mapping of the
236 flood impacts was also undertaken more widely in the systems to provide context for the analysis.
237 Methods applied are similar for each site.

238 Crest stage recorders have been used to measure peak flow stage (Hooke, 2007) during the study
239 period. These comprise water-sensitive tape, protected inside a tube, which changes colour when
240 washed by water. In very high flows the concreted installation can be washed away, but in these

241 cases channel flood marks are clear and are surveyed to obtain peak stage. Peak discharge is
242 calculated from detailed cross section surveys made with dGPS (Topcon HiperPro in recent years)
243 using the flood marks in that section and estimates of roughness using Manning's *n* coefficient,
244 mostly using a roughness coefficient of $n = 0.04$, assessed from the morphological and vegetation
245 characteristics of the reach but adjusted using the Lumbroso and Gaume (2012) method for high
246 Froude numbers. For the 2012 event, calculations of peak discharge have been made for each cross
247 section using pre- and post-flood morphology and using minima and maxima flood marks and flood
248 surface slope. These produce a range of estimates and indicate the associated uncertainty (Fig. 3B),
249 but the most likely value has been assessed from convergence within a site, most reliable flood
250 marks, and representative slope. Flow calculations do not incorporate possible changes from scour
251 and fill within the event or the effect of high sediment concentrations. Calculations of flow have also
252 been made using HEC-RAS (4.1.0) in each reach. Additional cross sections were also surveyed
253 between the monitored sites and have been combined with measurements from Kirkby and Smith
254 (Leeds University) to calculate the overall dynamics of the flood (Kirkby et al., 2013, Fig. 3B). No
255 duration data are available for the sites because no continuous recorders are in operation, but
256 duration data are available for the CHS gauges on the Nogalte at Puerto Lumbreras and on the
257 Guadalentín at Lorca
258 (http://www.chsegura.es/chs/cuenca/redesdecontrol/SAIH/visorsaih/visorjs.html). The Guadalentín
259 is a much larger system, to which the Torrealvilla is a tributary; but because of dams upstream, the
260 Torrealvilla must have contributed a large proportion of the flow at Lorca.

261 Morphology of the sites has been surveyed regularly and after flows using dGPS. The survey strategy
262 entails measurement of all bank lines and major features, retained as break lines in DEM
263 construction, and other points distributed over the surface of channels, bars, and floodplain in
264 proportion to the relief variability (a protocol established in 1996 but in line with subsequent
265 recommendations). In addition, cross sections are surveyed as these are best for detection of small
266 changes and are used for the discharge calculations.They are used for most of the analysis as

267 changes are highly accurately detected by exact repeat surveys using RTK GPS and as each can be
268 related to hydraulics at that section; they also illustrate the variability within reaches. A few
269 additonal cross sections were surveyed after the flood to aid in overall discharge calculation using
270 HEC-RAS. Long profile of the thalweg is also surveyed in each reach routinely. All points are
271 surveyed to an accuracy of ±2 cm. All the sites had been recently surveyed prior to the 2012 flood
272 (all checked or surveyed in January 2012) and after the most recent prior flow (mostly 2011).
273 Changes in cross section parameters (width, depth, area, *W/D*) and maximum erosion and
274 deposition in different zones (channel, bars, and floodplain) are measured by comparison of the
275 profiles. Gross amounts of erosion and deposition (cut and fill) in cross sections have also been
276 calculated using WinXSPRO. Cross section area has been calculated in relation to the 2012 flood
277 level, equivalent to flood capacity, and for bankfull level, assessed from the pre-flood morphology
278 and data on flow frequency (Hooke and Mant, 2015). The DEMs have been constructed using ArcGIS
279 software, incorporating break lines and using the TIN algorithm to retain points. Pre- and post-flood
280 DEMs have been compared to produce 'Difference of DEMs' (DoDs) of morphological changes, as in
281 the analysis of the 1997 flood (Hooke and Mant, 2000). The 'Geomorphological Change Detection'
282 plug-in (GCD 6) procedures attached to ArcGIS have been used to calculate net sediment volume
283 changes and uncertainties.

284 At each site quadrats were also established for measurement of vegetation and of sediment particle
285 size (Hooke, 2007). The vegetation quadrats are 3 m square and located in each representative zone,
286 i.e., channel, bars, and floodplain. The sediment quadrats are 0.5 m square and are located within
287 the vegetation quadrats. Sediment state is recorded by digital photography from which
288 measurements of size and detection of movement of particles can be applied. Sediment and
289 vegetation changes are not analysed in detail in this paper as they merit greater analysis than space
290 allows and because the focus here is on morphological changes, but some context is provided.

The relations of morphological change to the peak flow hydraulics, calculated from the cross section profiles using the slope-area method and HEC-RAS, and to preexisting morphology and conditions have been analysed graphically and quantitatively. They have been tested for relation of a range of parameters of change to magnitude of the flood (peak discharge and stream power) and to scale of forces (velocity, shear stress, and unit stream power) and for relation of amount of change to channel size and shape (width, depth, cross-sectional area, and *W/D*). Major parameters of change used include cross section capacity (area) change, net area change, maximum erosion, and deposition. Changes in all morphological parameters were tested but some were insensitive, with negligible changes so are not included in tables and graphs. Area change is equivalent to flood capacity and has been measured as the area under the 2012 flood level and for bankfull level, before and after the flood, and then the difference calculated. Net area change is the difference in the cross-sectional profile so it is equivalent to the amount of erosion and deposition in a cross section, gross change being the total of erosion and deposition, and the net change being the difference between total erosion and deposition.

## 4. Results

Figure 2 illustrates before and after flood states of each of the channel sites. For each of the six sites (Nog 1, Nog 2, and Nog Mon in Nogalte, and Oliva, Aqueduct, and Pintor in Torrealvilla) the changes in cross-sectional morphology, long profile of the thalweg, and the DEMs are analysed to quantify amount of change and to assess distribution and variability within the sites (Figs. 4-9). The overall changes in morphology as calculated by differences of pre- and post -flood DEMS (DoDs) are shown in Figure 10. The peak hydraulic conditions for cross sections are presented in Table 2 and the amounts of change measured on cross sections are given in Table 3. Changes from the sites are analysed in relation to the hydraulics of the flow, calculated from the cross sections and

315 measurement of flood stage, and to the preexisting morphology. Post-flood sediment characteristics
316 are indicated in Table 4.

317 *4.1. Nogalte sites*

318 ***Nog1.*** Prior to the flood this small channel in the headwaters of the Nogalte (CA 6.9 km $^2$) was 3-11
319 m wide at bankfull and only ~0.4 m deep (Fig. 2A). It is confined by steep slopes, with bedrock
320 outcropping in the valley sides. The reach is located 500 m downstream of a check dam, which
321 overtopped but remained intact in the September 2012 flood. Prior to that, hardly any channel flow
322 had occurred since 2003 and only very small flows in the period 1996-2003 (Hooke and Mant, 2015).
323 The inner (low flow) channel was poorly defined and the stream slightly braided, with vegetation on
324 some of the bars. The downstream end of the reach has a much steeper gradient than the upper
325 part.

326 The flow on 28 September 2012 reached 1.2 m stage on the crest stage recorder (which was bent
327 but not completely removed), and a flood width averaging 25 m. Repeat surveys were made on
328 three cross sections, and two additional cross sections were surveyed after the flood. Calculations of
329 the peak discharge produced a range of 37-56 $m^3 s^{-1}$; HEC-RAS modelling produced a range of 30-55
330 $m^3 s^{-1}$ for the surveyed flood elevations. Peak velocity was 3.5 m $s^{-1}$ and unit stream power 919 W
331 $m^{-2}$ (Table 2). In the upper, low gradient part, no incision occurred; but deposition of 3.27 $m^2$ and
332 maximum depth of 0.42 m occurred at X3, decreasing the flood capacity by 24% (Fig. 4). Farther
333 downstream the inner channel splits in two and both were incised in the flood, with increasing
334 amounts as the slope steepens from XCR to X10 (Fig. 4). These inner channels are 2-3 m wide and
335 0.5-0.6 m deep, with minor head cuts at the upstream end. The maximum erosion on a cross section
336 was 0.64 m and gross area of erosion 2.3 $m^2$. Depth increased by up to 19% of bankfull level and the
337 flood capacity increased by 12% at X10. The long profiles indicate net erosion throughout the
338 downstream part but some aggradation in the thalweg in the upstream part (Fig. 4). Two distinct
339 steps were present after the flood, one a previous step in hardened bed sediment that became

accentuated and the other a new head cut at the upstream end of the now distinct second channel on the bar (Fig. 10A). Maximum incision was 0.3 m. Overall, the flow increased the relief of the channel within the reach, both longitudinally and laterally. Net deposition of 108 ±40 $m^3$ (37% error) occurred within the reach, with 164 ±20 $m^3$ erosion and 272 ±35 $m^3$ deposition.

Sediment deposited was mostly fine gravel, typical of this channel (Table 4); but particles of 60-120 mm were deposited within the Retama and occasionally on bars, and particles up to 300 mm were found, trapped by vegetation. The higher bar areas were occupied by mature *Retama spp.* prior to the flood. These were severely damaged and flattened but not removed.

***Nog2.*** The second monitored reach downstream comprises a very wide, braided, active channel, with a main channel that crosses from the left to right side at the upstream end, but with multiple minor channels across the bar surfaces (Fig. 5). Prior to the major flood, only minor flows had occurred in the preceding 15 years, with none reaching the bar surfaces (Hooke, 2015a). The active channel occupies much of the valley floor but is bounded on both sides by earth embankments and agricultural terraced fields. The overall channel averages 70 m width and prior to the flood overall lateral relief was just <1 m. The flood reached 2.13 m height on the crest stage position though the instrument was removed. Discharge estimates are in the range 322-547 $m^3 s^{-1}$ but mostly near the latter, and this is the most probable value. The HEC-RAS modelling using a discharge of 500 $m^3 s^{-1}$ gives flood elevations very comparable to those surveyed, except at the downstream end in the steeper part. Peak velocity was calculated at 4 m $s^{-1}$ and maximum unit stream power as 1444 W $m^{-2}$.

At X1 (Fig. 5) at the upstream end, lateral enlargement of the main channel took place, removing the highest part of the bar surface. Deposition occurred on the left, distal side over a minor channel, forming a new upper bar. No bank erosion occurred. Cross section 2 was formerly a fairly even cross section with two channels, but they enlarged to become one major channel on the right and also incised by 0.4 m. Significant deposition of 0.3-0.8 m produced a high, even bar on the left. No bank erosion occurred, but deposition was evident on the field beyond the left embankment. Similarly,

365 on X3 (Fig. 5) the main channel enlarged and deepened and a new, small channel eroded in the
366 upper bar. Again, deposition produced a very even bar surface on the left. Bank erosion of 1.7 m
367 laterally occurred. At the downstream end at the crest recorder cross section (XCR; Fig. 5), the main
368 channel was much enlarged and deepened. Massive deposition occurred on the bar, the
369 combination producing much greater relief across the active channel - a change from 0.5 to 1.3 m.
370 The left bank bench was eroded.

371 Overall, little change in active width took place but up to 24% increase in maximum flood depth,
372 though 37% decrease in mean bankfull depth (taken as the inner channel). Net change in bankfull
373 channel area was up to -23% and in flood level capacity as much as -13% capacity. Maximum
374 erosion was -0.85 m and maximum deposition 0.85 m. Gross areas of cut were -13.9 $m^2$ at X3 and of
375 fill 20 $m^2$ at X1. Net aggradation was produced in all four cross sections. Maximum net change was
376 13.9 $m^2$ at X1, giving average deposition across the width of 18 cm. More deposition occurred in the
377 upstream end, with shallower gradient. The post-flood DEM (Fig. 5) shows clearly the new
378 channelling by braid streams across the main upper bar surface and accentuation of the main
379 channel. Minor head cuts were formed at the upstream end of the braid channels. The long profile
380 and DoD (Figs. 5, 10B) indicate net erosion along most of the main channel, except at the upstream
381 end, and a fairly uniform incision of 30 cm. Net deposition of 1111 ±148 $m^3$ (13% error) occurred
382 within the reach, with 1548 ±78 $m^3$ erosion and 2660 ±125 $m^3$ deposition.

383 Sediment deposited was mostly gravel (Table 4) but clasts up to 150 mm diameter were found in
384 remains of vegetation. At this site the sparse Retama were removed (or possibly buried in some
385 cases). Post-flood, the whole reach was almost entirely bare of vegetation, with just some remaining
386 stumps of Retama (Fig. 2A).

387 ***NogMon.*** The downstream reach, Nog Mon, is also a very wide braided site, of 120 m width (Fig. 6).
388 Prior to the flood it had a main low-flow channel on the left side of 0.5 m relief (Fig. 2A) and a more
389 minor, very shallow channel on the right hand side but numerous smaller braid channels across the

whole bar surface. Overall lateral relief was only 1 m. The channel is bounded on the left by a bedrock valley wall and on the right by an earth embankment with terraced fields beyond to the steep valley wall at a farther 50 m. The flood level reached a stage of 2.58 m equivalent on the crest stage recorder, though the equipment was completely removed. Peak discharge was calculated at ~820 $m^3 s^{-1,}$ excluding flow beyond the embankment; total flow exceeded 1000 $m^3 s^{-1}$. The HEC-RAS modelling for 800-900 $m^3 s^{-1}$ gave comparable heights at three post-flood cross sections. The flow just overtopped the embankment, but water also flowed downvalley through the fields from a tributary. Peak velocity was calculated at 4.7 m $s^{-1}$ and unit stream power at 1563 W $m^{-2}$.

On X1 (Fig. 6) almost the whole cross section underwent aggradation. Relatively deep deposition occurred on the entire right side up to a depth of 1 m. The main channel was narrowed by deposition in the original inner channel, but that was shifted to the left by bank erosion. Bank erosion of 1.8 m at 0.5 m height occurred in bedrock; but the total wedge removed was 3.5 m at the base and extended 1 m in height and about 4 m along the channel, thus equivalent to a bedrock volume of 10-12 $m^3$. Slight erosion was produced on the edges of the main bar area by secondary braid channels flowing off the bar. Similarly on X2 (Fig. 6) enlargement of the main channel took place but by lateral erosion of the bar rather than erosion of the solid valley wall margin and incision of 0.35 m. Massive deposition on the entire right side created a high, even bar. Cross-channel relief increased from 1 to 2.2 m. Some degradation of the right embankment took place. The thalwegs of both main channels are very uniform; but the left, more major channel, remained lower and deeper then the right side channel, as it had been prior to the flood. At the downstream end of the site the left bank was eroded, destroying a boquero channel that led through bedrock into fields (Hooke and Mant, 2002a) and the fields which it supplied were damaged.

Maximum change was up to 24% increase in flood level depth. The net change in bankfull area was a decrease of 48% to 63% and the decrease in flood capacity was 20%. Maximum erosion was -0.46 m and maximum deposition 0.91 m. Gross areas of change were -9.1 $m^2$ cut on cross profile X2

and 53.1 $m^2$ fill. Deposition averaged 0.44 m across the whole 120-m-wide channel. Overall, the braid pattern remained very similar to prior to the flood, with the main channels in a similar general position; but the reach experienced significant net aggradation and an increase in channel relief (Fig. 10C). Net deposition of 5648 ±235 $m^3$ (4% error) occurred within the reach, with 917 ±62 $m^3$ erosion and 6565 ±226 $m^3$ deposition.

Most of the deposits were fine gravel (Table 4); but occasional large cobbles of 100 mm were found and a very few blocks of 300 mm diameter, mainly trapped in the remains of vegetation. Prior to the flood much of the active channel was covered with mature Retama (Fig. 2A). Many of these were completely removed, some buried, and a few flattened but with some aerial parts still visible. On the right side of the valley the series of embanked fields fed by a cascade from the upper end and offtake from the main channel and a tributary were damaged, with embankments breached and destroyed. In the tributary upstream (Cardenas), a major check dam collapse occurred.

*4.2. Torrealvilla sites*

**Oliva.** This is the most upstream of the three measured reaches in the Torrealvilla catchment. It has a well-defined single channel, 8-10 m wide and 1m deep (Fig. 2B), set in a moderately wide valley with steep bedrock slopes and increasingly confined toward the downstream end. The floodplain is occupied by terraced and embanked almond and olive groves on the left side and tamarisk (*Tamarix canariensis)* bushes on the right side. Flood width varied from 43 m at the upstream end to 23 m at the downstream end. Flood level reached equivalent to 2.5 m on the crest stage though the instrument was removed (and found a few metres downstream). Peak flow is estimated at 110 $m^3 s^{-1}$ (though calculations vary between 77 and 148 $m^3 s^{-1}$ but with convergence of three out of five measurements). The HEC-RAS modelling using 100 $m^3 s^{-1}$ produced comparable flood elevations to

438 those surveyed. Peak velocity is calculated as 4.0 m $s^{-1}$ at the downstream end; unit stream power
439 ranges from 290 to 1381 W $m^{-2}$.

440 Five cross sections (CS) have been regularly surveyed in this site. All show incision in the flood but of
441 increasing amounts in the downstream direction (Fig. 7 with representative cross sections).
442 Negligible bank erosion occurred. Very little material was deposited on the floodplain, only veneers
443 in the open fields, and some mounds and wakes within the tamarisk vegetated zone. The long profile
444 is uniform in the upper two-thirds then steepens. Its form remained very similar but was incised
445 along the whole reach, with a greater steepening near the downstream end (Fig. 7). Changes in
446 morphology on cross sections were all small percentages of pre-flood size, with only one cross
447 section showing 14% increase in cross section area at flood level, but changes were up to 26% of
448 bankfull area. The maximum erosion was 0.56 m in the channel, and the maximum deposition 0.16
449 m on the floodplain. Net erosion of 636 ±79 $m^3$ (12% error) occurred within the reach, with 885 ±73
450 $m^3$ erosion and 248 ±30 $m^3$ deposition.

451

452 The channel bed is composed of coarse gravel (Table 4), but clasts up to 300 mm diameter are found
453 and were moved in the flow event. The channel has no vegetation. The dense tamarisk on the
454 floodplain was bent and damaged but not destroyed. The almond and olive trees on the floodplain
455 were not affected. Oleander (*Nerium oleander)* bushes on the channel banks were also not severely
456 damaged.

457 ***Aqueduct.*** This site is on the Prado tributary of the Torrealvilla and is a relatively active site in terms
458 of frequency of flow (Hooke, 2015a). It has a well-defined single channel 10-15 m wide and 0.8 m
459 deep (Fig. 2B) through most of the site but narrowing to 5 m and to 1.5 m deep at the downstream
460 end (Fig. 8). It is confined between steep valley walls with limited floodplain. Flood stage is of the
461 order of 3 m above the bed through most of the site. Discharge estimates range from 196 to 306 $m^3$

462 $s^{-1}$, but most likely estimates are around 270 $m^3$ $s^{-1}$, a value corroborated by estimates derived from
463 Structure from Motion analysis and two-dimensional flood modelling (Smith et al., 2014). Peak
464 velocity may have reached 4.7 m $s^{-1}$ at the downstream end and 1409 W $m^{-2}$ unit stream power.

465 Cross section comparison reveals channel morphology was only changed markedly in certain parts of
466 the reach (Fig. 8). In the upper part a bar was eroded and the channel widened, leading to
467 maximum vertical removal of 1.03 m. Elsewhere some slight channel incision occurred, but relatively
468 large amounts of material were deposited on the upper levels of the floodplain with maximum
469 deposition of 0.57 m. Some scouring of the thalweg of up to 0.5 m took place in the upstream part
470 and some fill in the lower part (Fig. 8), but all changes were complicated by some earlier human
471 impacts on the channel and floodplain in the central part. Mapping of an extended reach shows that
472 large changes took place at the downstream end of the reach, beyond the aqueduct structure, with
473 major scour holes excavated. Net erosion of 251 ±46 $m^3$ (18% error) occurred within the reach, with
474 656 ±36 $m^3$ erosion and 406 ±27 $m^3$ deposition, though this is somewhat influenced by human
475 impacts in the central part.

476

477 Sediment is mostly medium and coarse gravel but with finer and coarser patches (Table 4). They are
478 mostly thin veneers, with bedrock exposed in several places. The quadrat surveys show that fining
479 and coarsening took place as a result of the flood, and mapping showed patches varied slightly in
480 position. The channel is mostly not vegetated. The floodplain was occupied by grasses and low
481 shrubs and these were severely affected, exposing much more bare ground (Fig. 2B). Tamarisk
482 bushes were damaged but not removed.

483 ***Pintor.*** This is the downstream site on the main stem of the Torrealvilla and replaced a nearby site in
484 2002 (Hooke, 2015a). It has a single channel, 20 m wide, set between embankments separating off
485 fields and irrigation channels. It has a slightly more pronounced inner channel in the middle part (Fig.

2B). Measurement of flood levels indicates that the peak reached over 3.5 m above the crest recorder datum and overtopped the boquero wall (Fig. 9). Peak discharge is calculated as between 345 and 451 $m^3 s^{-1}$ with peak velocity of 4.2 m $s^{-1}$ and peak unit stream power of 942 W $m^{-2}$. The HEC-RAS produces rather lower estimates of peak flow (300-375 $m^3 s^{-1}$).

Almost no morphological change took place at the Pintor site, at least within the channel as registered on the cross sections. Maximum erosion was 0.39 m in one location. Thalweg scour of up to 0.25 m occurred in the upstream part and fill of a maximum of 0.20 m in the downstream part. The DoD reveals rather greater patchiness of change (Fig. 10F). Just upstream of the reach, in a section near a previously collapsed check dam, the configuration and depth of the scour holes was changed, as evident in the long profile (Fig. 9). Elsewhere, some degradation of the thalweg occurred but mostly aggradation, including infill of a major scour hole downstream. Net erosion of 208 ±40 $m^3$ (19% error) occurred within the reach, with 357 ±34 $m^3$ erosion and 149 ±20 $m^3$ deposition.

Some blocks up to 2 m in size, remains of a masonry check dam at the upstream end destroyed previously, were moved. Within the main reach the coarse gravel and cobble bed was mobilised but similar sizes redeposited (Fig. 2B; Table 4). The site is virtually devoid of vegetation within the channel. Tamarisk on the embankments was slightly damaged and bent. Material was deposited in the irrigation channel at 2 m above the channel, and a major breach in the left hand embankment took place.

### *4.3. Morphological change in relation to flood hydraulics and morphology*

The data on changes from all cross sections have been analysed in relation to the computed peak flow hydraulics (peak discharge, stream power, velocity, unit stream power, and shear stress) derived from the surveyed flood stages on each profile and to the pre-flood morphology (width, depth, and cross-sectional area). All the changes in cross-sectional area (flood capacity at 2012 flood

level) on the Nogalte exhibit a decrease because of aggradation except in one cross section. For flood level, changes in cross sectional area are near linear and just significant (at $p = 0.05$) in relation to discharge but have little relationship to any of the other hydraulic variables (Table 5). However, change in bankfull channel area shows a strong nonlinear relation and significant linear correlation to discharge and high linear correlations to stream power, unit stream power, and shear stress but lower correlation with velocity (Fig. 11; Table 5). Changes in average depth show considerable scatter and little consistent relationship to any hydraulic variables at either flood or bankfull level except for a significant relationship of change in bankfull depth to mean velocity (Table 5). Changes in morphology on the Torrealvilla are mostly small and show high variability to all hydraulic parameters at bankfull and at flood levels with no significant correlations (Fig. 11; Table 5).

Total net changes of cut-and-fill areas on cross sections on the Nogalte show positive relations to all hydraulic parameters, though the net change at the Nog 2 sites are rather lower than at the other sections (Fig. 12). The relationships to discharge and stream power are significant; but the relations to velocity, unit stream power, and shear stress are weak (Table 5). Gross cross section area change (cut and fill), which is a measure of extent of total reworking at a cross section, exhibits very high correlations to discharge and stream power and moderate relations to velocity, shear stress, and unit stream power for the Nogalte sites (all relations significant, Table 5). The gross amount of erosion on the Nogalte shows a weak relationship to velocity and unit stream power but insignificant relation to discharge, stream power, and shear stress. In contrast, for gross depositional area all relationships on the Nogalte are significant but especially strong for peak discharge and stream power (Table 5). Thus the changes in cross-sectional form on the Nogalte, which are mainly depositional, are closely related to the total flow and energy available and less strongly to the forces of flow. Some increase in channel capacity took place at the Torrealvilla sites; but the changes are all small compared with those for the Nogalte even for comparable values of the hydraulic parameters (Fig. 12). Correlations are obviously low (Table 5).

Maximum erosion shows no relationship to any of the hydraulic variables for the Nogalte nor for the Torrealvilla sites, which are dominantly net erosional (Fig. 13; Table 5). Maximum deposition exhibits more consistency in relationships, with the correlation to peak discharge and stream power being significant for the Nogalte (Fig. 13; Table 5). The Torrealvilla sites have lower values of deposition for equivalent values of velocity, shear stress, and unit stream power. Overall, relations for amount of deposition to hydraulic variables are much stronger than for measures of erosion, particularly for the Nogalte sites.

Analysis of morphological changes in relation to the pre-flood morphology indicates that, on the Nogalte, change in cross-sectional capacity at bankfull level exhibits a moderate scaling to size of channel (width, depth) and a moderate relationship also to *W/D*. At flood level the relationships to width and *W/D* are significant but not that to depth (Fig. 14A; Table 5). Changes in capacity on the Torrealvilla are all small and insignificant. Changes in depth are significantly related to average depth for the Nogalte sections at bankfull level. Net changes in cross-sectional area, gross changes, and gross depositional changes all have high correlations with width, cross sectional area of the channel, and *W/D* ratio but not to depth on the Nogalte (Table 5). Conversely, gross amount of erosion is related to depth but not other morphological variables. Maximum erosion in cross sections exhibits some inverse relation to depth but otherwise large scatter to channel size parameters and lack of relation to preexisting channel size or morphology, but the maximum deposition has significant relationships to width, depth, and area (especially width), indicating a general scaling relationship (Fig. 14B). The Torrealvilla sites are much less consistent, and all changes are insignificant except maximum deposition to *W/D* ratio. Gradients are not sufficiently varied to test relations.

## 5. Discussion

559 The major changes that occurred on the Nogalte at the measurement sites were large amounts of
560 aggradation and accentuation of the cross-channel relief by some slight scour of inner channels but
561 high deposition on bars and floodplains. In the much lesser flood on the Torrealvilla, the effects
562 were smaller and more variable but mostly erosional in the channels and depositional on the
563 floodplains at the monitored sites. At none of the monitored sites did the morphology change
564 radically in type, for example from meandering to braided, nor did very large scour holes or major
565 longitudinal changes take place. This is not simply a reflection of selection or position of the
566 monitored reaches because mapping of morphological changes all down the main channels
567 identified that these were the predominant types of changes. However, elsewhere on the Nogalte
568 some chute channels were cut on bends, though the outer channel remained the main channel. In
569 some locations major bank erosion occurred, particularly in narrower sections and at the
570 downstream end of the channel (nearer to Puerto Lumbreras) where the end of a track was
571 severed, a road and reinforced slope severely undercut, and field bank structures eroded. The flood
572 was capable of eroding bedrock valley walls, as evidenced at NogMon site (Fig. 10C, left bank on the
573 DoD) and downstream. In the Nogalte, because of the even channel gradient and the lack of
574 bedrock exposures in the channel except near the upstream end, marked headcuts are not a feature
575 of the main channel. Small-scale features did occur in the braid channel heads on bars and major
576 gullying with headcuts did occur where the chute cutting took place on bends, exterior to the
577 monitored reaches. Even on the Torrealvilla, where scour holes and head cutting occurred in the
578 1997 flood (Hooke and Mant, 2000) this was much less common in this event, in spite of flow at
579 Prado (Aqueduct) being more than twice that of 1997. Some significant changes, mainly incision, did
580 take place upstream in Prado beyond the monitored reach. Overall on the Nogalte, large amounts of
581 deposition occurred and channel morphology was modified in braided sections, but qualitative
582 change in morphology of channels did not occur. This event in the Nogalte would therefore be
583 classified as high magnitude in Wolman and Miller's (1960) terms of sediment transport but
584 relatively low in terms of flood effectiveness (Wolman and Gerson, 1978). The Nogalte channel could

585 be regarded as robustly adapted to large events, i.e., adjusting with events but not crossing
586 thesholds (Werritty and Leys, 2001).
587
588 Various definitions exist in the literature on the classification and limits for various types of flood
589 including large, extreme, and catastrophic (Hooke, 2015b). Machado et al. (2011) analysed rainfall
590 events in SE Spain, including in the Guadalentín, and classified relative magnitude of flood according
591 to impacts: 1. ordinary: discharge contained within channel and banks; 2. extraordinary: localised
592 overbank flow with resulting damages but no major destruction; and 3. catastrophic: floodplain
593 flooding and general damage and destruction of infrastructure. They classed the 1973 flood at Lorca
594 as catastrophic, and in their terms this flood on the Nogalte would be catastrophic. Conesa García
595 (1995) produced a fourfold classification, combining flow levels and effects. Others have mostly
596 applied the term catastrophic to dam burst, glacial floods, and proglacial jökulhlaups with very major
597 impacts. The 2012 event is not overall assessed as catastrophic from the evidence assembled here.
598 However, some of the hydrological characteristics, such as the rate of rise and the unit discharge
599 would appear to be very high on world scales. For example, if compared with Costa's (1987)
600 envelope curve of discharge in relation to catchment area and Thompson and Croke's (2013) plot of
601 Australian floods on the same graph, this flood plots on the upper edge of the distribution of points
602 (Fig. 15); it would therefore appear to be an extreme hydrological event. The unit stream powers in
603 relation to catchment area are also high in Magilligan's (1992) distributions and exceed his 300 W $m^{-2}$
604 for major change. The flood on the Nogalte had at least a 50-year RI and possibly much rarer than
605 that as indicated by the rainfall calculations (Kirkby et al., 2013) and by older irrigation structures in
606 the sides of channels that were destroyed. However, several events that produced casualties are
607 recorded for the 1980s in SE Spain (Barredo, 2007). The flow on the Nogalte in 2012 has been
608 measured at the CHS gauge as much higher than the disastrous 1973 event (because the market was
609 in progress in the channel), though available figures for that range from 1100 to 2000 $m^3 s^{-1}$. The
610 maximum rainfall in 2012 was possibly not as high as in 1973; but in 2012 the rainfall covered the

611 whole catchment, whereas in 1973 it was confined to the upper part whilst the lower part remained
612 dry. Detailed data of morphological impacts are not available for 1973. Conesa García (1995)
613 recorded several events in the Nogalte in the 1980s that produced significant morphological changes
614 and deposits of similar form to the present, including a lack of stable areas, large bar deposition, and
615 erosion only in braid channels. The 2012 event was at least 20 times larger then the largest event
616 he measured. Extrapolation of a 10-year rainfall record in the Torrealvilla area (Bracken et al., 2008)
617 produces a recurrence interval for the event rainfall there of ~100 years (Smith et al, 2014).

618

619 The previous highest flow at these sites was in 1997, an event that was also measured and
620 documented in detail (Hooke and Mant, 2000). In that case the flow was higher on the Torrealvilla
621 than the Nogalte. The 2012 flood on the Torrealvilla was almost exactly the same discharge as the
622 1997 flood at Oliva but much higher than 1997 at Aqueduct and Pintor (replacement of Serrata).
623 Major changes took place in 1997 on the Torrealvilla, including formation of major scour holes and
624 some deposition on the floodplains. At Oliva the channel morphology was changed markedly with
625 incision of a very shallow channel. On the Nogalte, no flow at all occurred in 1997 at Nog 1 and Nog
626 2, and flow of 0.55 m at Nog Mon (compared with 2.58 m in 2012). A regression equation fitted to
627 the maximum erosion data in relation to peak discharge for the 2012 event in the Torrealvilla
628 produces a much lower gradient trend line and a much lower correlation ($b$ = 0.0029, $r^2$ = 0.403)
629 compared with that for the 1997 event ($b$ = 0.008, $r^2$ = 0.769) for the same sites (Hooke and Mant,
630 2000). The morphology and coarse sediment calibre at Oliva and at Pintor are thought to have
631 produced high resistance to change in the 2012 flood, and feedback effects of the altered
632 morphology from the 1997 event increased resistance to change (Hooke, 2015b). Occurrence of
633 scour holes and of major rilling and gullying overall was not all that evident in this flood event and
634 this may be related to the rapid onset and the dry state of the ground at the time and to the
635 widespread runoff. Unlike the 1997 event (Bull et al., 1999), the 2012 flood event was preceded by
636 very hot, dry conditions and no preceding channel flow. These sites have been monitored now for up

637 to 18 years, and an assessment of the overall contribution of these major flood events and of more
638 minor flows and their sequences reveals that 70-85% of the total change in cross sections as
639 measured at NogMon in that period took place in the 2012 event, whereas it was a much lower
640 proportion at the Torrealvilla site where change events have been more frequent and the 2012 was
641 of lower relative magnitude (Hooke, 2015a).
642
643 The results of analysis of relationships of morphological changes to hydraulics and morphological
644 variables indicate that magnitude of the changes in the 2012 event is generally scaled to discharge
645 and flood channel size, width and cross-sectional area, and shows less relation to depth of channel
646 (Table 5). On the Nogalte total activity as measured by gross changes in cross sections (i.e., cut and
647 fill) is very highly correlated to discharge and stream power and also to size, as measured by flood
648 width and cross-sectional area. Thus a scaling of activity and especially deposition with the flood
649 magnitude and the size of channel is apparent, indicating capacity to carry sediment and space for
650 deposition were key controls. Most of the Nogalte course is of uniform gradient (Hooke and Mant,
651 2002b) so no major zones of lower slope are present to induce deposition. Channel width is the
652 major morphological influence. Maximum erosion exhibits no relation to any hydraulic parameters.
653 Maximum deposition, by contrast, is again related to peak discharge and stream power, so volume
654 of water and total and energy of flow, but it is not related to measures of force of flow, velocity,
655 shear stress, or unit power. Likewise, gross erosion and maximum erosion are more related to
656 measures of forces in the flow and also to depth than to total discharge or stream power, whereas
657 for gross deposition this is reversed. This could be a reflection that a certain force is needed to
658 achieve erosion but, on the other hand, peak forces at most cross sections were in excess of erosion
659 thresholds. It is suggested that these outcomes are closely related to the event characteristics (see
660 below) but also to the sites.

661 In terms of sites, the discharge and stream power values were much higher on the Nogalte than at
662 the Torrealvilla sites, reflecting the much greater flow magnitude; but the range of velocity, shear

663 stress, and unit stream power values of the two sets of sites overlap in the lower part of the range.
664 The changes produced by comparable values of these variables are greater on the Nogalte sites than
665 on the Torrealvilla (Fig. 13). This could be because of differences in resistance and density of the
666 materials. The Nogalte channel is mostly a broad braided channel composed of extremely loose and
667 friable gravel (Table 4) that is very easily mobilised. The marl channels of the Torrealvilla are more
668 resistant with more coarse material but also more cohesive silt and clay in the fine material (Table
669 4). This influences the type of morphology but also the sediment supply and transport dynamics
670 within the event.

671 In terms of the event characteristics, much field evidence such as from channel deposits, tributary
672 fans, and sediment filling of structures points to extremely high sediment supply and sediment flux
673 in the Nogalte event and very high connectivity within the system. The lack of net erosion on the
674 Nogalte may be because the stream was carrying sediment at capacity very quickly after the start of
675 the event from the upstream end right through the system owing to the high supply from the bare
676 slopes under almonds and rapid mobilisation of the channel bed, the very high runoff per unit area,
677 the very sudden rise in discharge (1 h to peak of 2500 $m^3 s^{-1}$ at Puerto Lumbreras at the downstream
678 end), and the short duration of the event. Also, the Nogalte has deep deposits on the bed of the
679 channel in the downstream sites. Scour can take place in events before fill, as is well known in
680 ephemeral channels, and it is likely that a depth of the bed was mobilised very rapidly. Pits dug at
681 the NogMon site indicate from the stratigraphy of the sediment and from evidence of exposed then
682 buried plant roots that scour and mobilisation took place to a depth of at least 20 cm and possibly 60
683 cm even in the lowest elevation parts. More detailed analysis of the sediment dynamics and
684 mechanics of transport is being undertaken. Flows on the Nogalte were possibly non-Newtonian.

685 That the major deposition was on the higher parts of bars and floodplains may also be a reflection
686 of the dynamics of the event, with peak sediment load occurring early in the event at most sites. The
687 major deposition on the Nogalte was mostly as very flat, even bars, occupying a large proportion of

688 the active channel width. These are very similar to those described by Billi (2008) in channels of the
689 Kobo basin in northern Ethiopia and are considered consistent with Froude numbers near transition
690 leading to formation of plane beds, Many of the Froude numbers calculated for sections in the
691 Nogalte at peak flow were approaching or exceeded a Froude value of 1 (Table 2). This reinforces the
692 hypothesis of major deposition near the event peak.

693

694 Debate has surrounded whether flood impacts tend to be most closely related to peak discharge, to
695 duration, or to measures of force such as unit stream power (Hooke, 2015b). Magilligan (1992)
696 argued that 300 W $m^{-2}$ represents a threshold value for occurrence of major morphological changes.
697 Peak unit stream power at all the Nogalte sections (except Nog 1 X1, the uppermost section)
698 exceeded that, some of them by a large amount (Table 2). Similarly, on the Torrealvilla all sites
699 exceeded the threshold except X2 (very close) and X5 at Oliva. Major morphological change might
700 therefore have been expected. The ranges for the Nogalte shear stress and stream power per unit
701 boundary area were 100-364 N $m^{-2}$ and 285-1563 W $m^{-2}$, respectively. These compare with values of,
702 for example, 87-398 N $m^{-2}$ and 212-2134 W $m^{-2}$ found by Grodek et al. (2012) for a flood in Israel,
703 which were higher than any other recorded floods in the Mediterranean climatic region of Israel,
704 and produced significant landform changes. However, Heritage et al. (1999) and Nardi and Rinaldi
705 (2015) found less morphological effect from major flood events than anticipated by calculation of
706 hydraulics and relations to published thresholds and sediment transport equations. Lack of
707 consistency in relationships is also common to many ephemeral channels. Hooke (2015b) has
708 discussed the multiple factors that can affect the geomorphological impact of an event.

709 Some major effects on infrastructure took place, including destruction of check dams, field
710 embankments and terrace systems, erosion of banks and bank protection, damage to boqueros and
711 irrigation systems, and erosion of tracks. Within the region, a motorway bridge across a channel
712 collapsed. Overall, the morphology of these channels is adapted to flash floods of high magnitude

except where constrained by structures. This event indicates the magnitude of impacts to be expected and that need to be allowed for in management, especially as their occurrence is predicted to increase under climate change and land use scenarios.The presence of check dams, which mostly stayed intact, reduced the peak flows (CHS); and additonal dams have since been built in the Nogalte to increase water retention even more. Flood capacity at flood level decreased by up to 25% in the Nogalte sites and probably similarly along much of the course, which has implications for future flood management in this currently rapidly aggrading course. Flow capacity for inner channels at bankfull level was also decreased, but bar areas were raised so are less likely to be inundated, which has implications for vegetation growth. These channels are mostly still relatively unconstrained and unengineered except for check dams and crossings, but Ortega et al. (2014) demonstrated the consequences if morphological and sedimentary adjustments are not allowed for from high magnitude floods. Strategies need to allow for the channel changes, and this is beginning to be recognised in such ideas as 'minimum morphological spatial demand of rivers' (Krapesch et al., 2011) or 'freedom space' of rivers (Biron et al., 2014), though advocated long ago (Hooke and Redmond, 1989). The Nogalte is typical of a certain type of semiarid region, ephemeral stream that is wide and braided in much of its course but flows in a well-defined valley in high relief, has a loose, fine gravel bed that is highly mobile, and where major flows are infrequent. These channels are well adapted to high magnitude events.

## 6. Conclusions

A flash flood event occurred in SE Spain on 28 September 2012 and affected channel reaches on the Nogalte and Torrealvilla streams that were being monitored to measure effects of flows. The flood was of very high magnitude and could be classed as extreme on the Nogalte as judged by its peak discharge in relation to catchment area, compared with other published values on a world scale. It had a particularly high rate of rise of 2500 $m^3 s^{-1}$ in an hour at the downstream end. It is estimated

to have a recurrence interval of at least 50 years but could be much greater. The event produced casualties and damage to infrastructure. However, the geomorphic impacts were not as high as might be anticipated from the calculated unit stream power and shear stresses. The main effects were a high mobilisation of sediment that produced large amounts of deposition in the form of high, flat bars in the mainly braided channel and net aggradation in the monitored reaches. Some limited erosion occurred in low flow channels, the combination resulting in an increase in cross-channel topographic relief. The flood occupied much of the valley floor, but channel pattern was not markedly changed. Bedrock erosion of the valley wall did occur in some locations. The high availability of sediment on the slopes and in the channels, the rapid sediment mobilisation from the extreme rate of hydrograph rise, and the short duration of the flash flood probably prevented much erosion except at some margins. Analysis of amounts of change in channel morphology in relation to hydraulic parameters of the flow indicate a strong relationship of gross amounts of change and of deposition to size of channel, mainly width, and of amounts of deposition to peak discharge and stream power but weaker relations to measures of force of peak flow. Erosional changes showed little relationship to hydraulics of channel morphology. A lower magnitude flow in the neighbouring catchment, Torrealvilla, produced more varied changes and rather less impact in many locations than an event measured in 1997. The amount of change resulting from comparable flow forces on the Torrealvilla marl channel was less than that on the Nogalte channel composed of loose schist gravel. These channels, where not constrained by structures, are adapted to such flash floods; but floods of such magnitude need to be allowed for in management of the channel and catchment.

**Acknowledgements**

I should like to thank Robert Perry for assistance with the fieldwork and data processing, Mark Smith and Mike Kirkby (Leeds) for use of additional discharge estimates in the Nogalte (Fig. 3B), Aleix Calsamiglia for GIS assistance, and Suzanne Yee for drawing the diagrams.

763

764 **References**

765 AON Benfield, 2012. September 2012 Global Catastrophe recap. <http://
766 thoughtleadership.aonbenfield.com/Documents/20121004_if_global_cat_recap_
767 september.pdf> (Date Accessed: 14.05.14).
768 Arnaud-Fassetta, G., Ballais, J.L., Begnin, E., Jorda, M., Meffre, C., Provansal, M., Roclitis, J., Suanez,
769 S., 1993. La crue de l 'Ouveze á Vaison-la-Romaine _22-9-92: Ses effets morphodynamiques,
770 sa place dans le fonctionnement d'un géosystème anthropisé. Revue de Géomorphologie
771 Dynamique XLII, 34–48.
772 Baker, V. R., Costa, J. E., 1987. Flood Power. In: Mayer, L., Nash, D. (Eds.), Catastrophic Flooding.
773 Allen and Unwin, Boston, pp1-21.
774 Barredo, J.I., 2007. Major flood disasters in Europe: 1950–2005. Nat. Hazards 42, 125–148.Batalla, R.
775 J., García, C., Balasch, J. C., 2005. Total sediment load in a Mediterranean mountainous
776 catchment (the Ribera Salada River, Catalan Pre-Pyrenees, NE Spain). Zeitschrift für
777 Geomorphologie 49, 495-514.
778 Billi, P., 2008. Bedforms and sediment transport processes in the ephemeral streams of Kobo basin,
779 Northern Ethiopia. Catena, 75, 5-17.
780 Biron, P.M., Buffin-Bélanger, T., Larocque, M., Choné, G., Cloutier, C. A., Ouellet, M. A., Demers, S.,
781 Olsen, T., Desjarlais, C., Eyquem, J., 2014. Freedom space for rivers: a sustainable
782 management approach to enhance river resilience. Environmental Management 54, 1056-
783 1073.
784 Bracken, L. J., Cox, N. J., Shannon, J., 2008. The relationship between rainfall inputs and flood
785 generation in south-east Spain. Hydrological Processes 22, 683-696.
786 Brookes, C. J., Hooke, J. M., Mant, J.M., 2000. Modelling vegetation interactions with channel flow in
787 river valleys of the Mediterranean region. Catena 40, 93-118.

788 Bull, L. J., Kirkby, M. J., Shannon, J., Hooke, J. M., 1999. The impact of rainstorms on floods in
789 ephemeral channels in southeast Spain. Catena 38, 191-209.
790 Cenderelli, D. A., Wohl, E. E., 2003. Flow hydraulics and geomorphic effects of glacial-lake outburst
791 floods in the Mount Everest region, Nepal. Earth Surface Processes and Landforms 28, 385-
792 407.
793 CHS Confederación Hidrográfica del Segura.
794 https://www.chsegura.es/chs/cuenca/redesdecontrol/SAIH/ .Website accessed February
795 2015.
796 Cohen, H., Laronne, J. B., Reid, I., 2010. Simplicity and complexity of bed load response during flash
797 floods in a gravel bed ephemeral river: A 10 year field study. Water Resources Research 46.
798 Conesa-García, C., 1995. Torrential flow frequency and morphological adjustments of ephemeral
799 channels in south-east Spain. In: Hickin, E. J. (Ed.), River Geomorphology. Wiley, Chichester,
800 171-192.
801 Coppus, R., & Imeson, A. C., 2002. Extreme events controlling erosion and sediment transport in a
802 semi-arid sub-andean valley. Earth Surface Processes and Landforms, 27, 1365-1375.
803 Costa, J.E., 1987. A comparison of the largest rainfall-runoff floods in the United States with those of
804 the Peoples Republic of China and the world. J. Hydrol. 96, 101–115.
805 Costa, J.E., O'Connor, J.E., 1995. Geomorphically effective floods. In: Costa, J.E., Miller, A.J., Potter,
806 K.W., Wilcock, P.R. (Eds.), Natural and Anthropogenic Influences in Fluvial Geomorphology
807 (The Wolman Volume). American Geophysical Union, Washington D.C., pp89–104.
808 Croke, J., Fryirs, K., Thompson, C., 2013. Channel-floodplain connectivity during an extreme flood
809 event: implications for sediment erosion, deposition, and delivery. Earth Surface Processes
810 and Landforms 38, 1444-1456.
811 Dean, D. J., Schmidt, J. C., 2013. The geomorphic effectiveness of a large flood on the Rio Grande in
812 the Big Bend region: Insights on geomorphic controls and post-flood geomorphic response.
813 Geomorphology 201, 183-198.

814 Fuller, I. C., 2008. Geomorphic impacts of a 100-year flood: Kiwitea Stream, Manawatu catchment,
815 New Zealand. Geomorphology 98, 84-95.
816 Gaume, E., Bain, V., Bernardara, P., Newinger, O., Barbuc, M., Bateman, A., Blaskovicova, L.,
817 Bloeschl, G., Borga, M., Dumitrescu, A., Daliakopoulos, I., García, J., Irimescu, A., Kohnova, S.,
818 Koutroulis, A., Marchi, L., Matreata, S., Medina, V., Preciso, E., Sempere-Torres, D., Stancalie,
819 G., Szolgay, J., Tsanis, I., Velasco, D., Viglione, A., 2009. A compilation of data on European
820 flash floods. Journal of Hydrology 367, 70-78.
821 Greenbaum, N., Bergman, N., 2006. Formation and evacuation of a large gravel-bar deposited during
822 a major flood in a Mediterranean ephemeral stream, Nahal Me'arot, NW Israel.
823 Geomorphology 77, 169-186.
824 Grodek, T., Jacoby, Y., Morin, E., Katz, O., 2012. Effectiveness of exceptional rainstorms on a small
825 Mediterranean basin. Geomorphology 159–160, 156-168.
826 Grove, J. R., Croke, J., Thompson, C., 2013. Quantifying different riverbank erosion processes during
827 an extreme flood event. Earth Surface Processes and Landforms 38, 1393-1406.
828 Harvey, A. M., 1984. Geomorphological response to an extreme flood: a case from southeast Spain.
829 Earth Surface Processes and Landforms 9, 265-279.
830 Hauer, C., Habersack, H., 2009. Morphodynamics of a 1000-year flood in the Kamp
831 River, Austria, and impacts on floodplain morphology. Earth Surface Processes
832 and Landforms 34, 654–682.
833 Heritage, G. L., Birkhead, A. L., Broadhurst, L. J., Harnett, B. R., 1999. The influence of flooding on
834 the erodibility of cohesive sediments along the Sabie River, South Africa. In: International
835 Association of Sedimentologists Special Publication 28, Blackwell, Oxford, pp131-145
836 Herrera, S., Fita, L., Fernandez, J., & Gutierrez, J. M., 2010. Evaluation of the mean and extreme
837 precipitation regimes from the ENSEMBLES regional climate multimodel simulations over
838 Spain. Journal of Geophysical Research-Atmospheres 115, Article Number: D21117.

839 Hooke, J. M., 2007. Monitoring morphological and vegetation changes and flow events in dryland
840 river channels. Environmental Monitoring and Assessment 127, 445-457.
841 Hooke, J.M., 2015a Morphological impacts of flow events of varying magnitude on ephemeral
842 channels in a semiarid region. Geomorphology
843 Hooke, J.M., 2015b Variations in flood magnitude-effect relations and the implications for flood risk
844 assessment and river management. Geomorphology doi:10.1016/j.geomorph.2015.05.014
845 Hooke, J. M., Mant, J. M., 2000. Geomorphological impacts of a flood event on ephemeral channels
846 in SE Spain. Geomorphology 34, 163-180
847 Hooke, J. M., Mant, J. 2002a. Floodwater use and management strategies in valleys of southeast
848 Spain. Land Degradation & Development, 13(2), 165-175.
849 Hooke, J., Mant, J., 2002b. Morpho-dynamics of ephemeral streams. In: Bull, L. J., Kirkby, M. J. (Eds.)
850 Dryland Rivers: Hydrology and Geomorphology of Semiarid Channels. John Wiley & Sons,
851 Chichester. pp. 173-204.
852 Hooke, J., Mant, J., 2015. Morphological and vegetation variations in response to flow events in
853 rambla channels of SE Spain. In: Dykes, A. P., Mulligan, M. and Wainwright, J. (Eds.),
854 Monitoring and Modelling Dynamic Environments (A Festschrift in memory of Professor John
855 B. Thornes). Chichester: John Wiley & Sons, pp 61-98.
856 Hooke J.M., Redmond C.E., 1989. River channel changes in England and Wales. Journal of Institution
857 of Water and Environmental Management 3, 328-335.
858 Hooke, J. M., Brookes, C. J., Duane, W., Mant, J. M., 2005. A simulation model of morphological,
859 vegetation and sediment changes in ephemeral streams. Earth Surface Processes and
860 Landforms 30, 845-866.
861 Huckleberry, G., 1994. Contrasting channel response to floods on the middle Gila River, Arizona.
862 Geology 22, 1083-1086.
863 Jansen, J.D., 2006. Flood magnitude–frequency and lithologic control on bedrock river incision in
864 post-orogenic terrain. Geomorphology 82, 39–57.

865 Kirkby, M., Hooke, J., Smith, M., Barberá, G., García-Pintado, J., Bracken, L., 2013. Hydrological
866 impacts of floods in SE Spain, September 2012. Poster paper at IAG International
867 Conference, Paris.
868 Kochel, R. C., 1988. Geomorphic impact of large floods: review and new perspectives on magnitude
869 and frequency. In: Baker, V. R. , Kochel, R. C., Patton, P. C. (Eds.), Flood Geomorphology.:
870 Wiley, New York, pp169-188.
871 Krapesch, G., Hauer, C., & Habersack, H., 2011. Scale orientated analysis of river width changes due
872 to extreme flood hazards. Natural Hazards and Earth System Sciences, 11(8), 2137-2147. doi:
873 10.5194/nhess-11-2137-2011.
874 Laronne, J.B., Reid, I. 1993. Very high-rates of bedload sediment transport by ephemeral desert
875 rivers. Nature 366 (6451), 148-150.
876 Lumbroso, D., Gaume, E., 2012. Reducing the uncertainty in indirect estimates of extreme flash flood
877 discharges. J. Hydrol. 414–415, 16–30.
878 Machado, M. J., Benito, G., Barriendos, M., Rodrigo, F. S., 2011. 500 years of rainfall variability and
879 extreme hydrological events in southeastern Spain drylands. Journal of Arid Environments
880 75, 1244-1253
881 Magilligan, F. J., 1992. Thresholds and the spatial variability of flood power during extreme floods.
882 Geomorphology 5, 373-390.
883 Mairota, P., Thornes, J. B., Geeson, N. A. (Eds.), 1998. Atlas of Mediterranean environments in
884 Europe: the desertification context. Wiley, Chichester, 224pp.
885 Martín-Vide, J.P., Ninerola, D., Bateman, A., Navarro, A., Velasco, E., 1999. Runoff and sediment
886 transport in a torrential ephemeral stream of the Mediterranean coast. Journal of Hydrology
887 225, 118–129.
888 Milan, D. J., 2012. Geomorphic impact and system recovery following an extreme flood in an upland
889 stream: Thinhope Burn, northern England, UK. Geomorphology 138(1), 319-328.

890 Miller, A. J., 1990. Flood hydrology and geomorphic effectiveness in the central Appalachians. Earth
891 Surface Processes and Landforms 15, 119-134.
892 Nardi, L., & Rinaldi, M., 2015. Spatio-temporal patterns of channel changes in response to a major
893 flood event: the case of the Magra River (central-northern Italy). Earth Surface Processes
894 and Landforms, 40, 326-339.
895 Navarro Hervás, F., 1991. El Sistema Hidrográfico del Gaudalentín. Region de Murcia, Murcia, 256 pp.
896 Newson, M., 1989. Flood effectiveness in river basins: progress in Britain in a decade of drought. In:
897 Beven, K., Carling, P. (Eds.), Floods: Hydrological, Sedimentological and Geomorphological
898 Implications. Wiley, Chichester, pp 151-170.
899 Nichols, M. H., Stone, J. J., Nearing, M. A., 2008. Sediment database, Walnut Gulch Experimental
900 Watershed, Arizona, United States. Water Resources Research, 44(5).
901 Ortega, J. A., & Garzón Heydt, G., 2009. Geomorphological and sedimentological analysis of flash-
902 flood deposits: The case of the 1997 Rivillas flood (Spain). Geomorphology 112, 1-14.
903 Ortega, J. A., Razola, L., & Garzon, G., 2014. Recent human impacts and change in dynamics and
904 morphology of ephemeral rivers. Natural Hazards and Earth System Sciences, 14, 713-730.
905 Poesen, J. W. A., Hooke, J. M., 1997. Erosion, flooding and channel management in Mediterranean
906 environments of southern Europe. Progress in Physical Geography 21, 157-199
907 Powell, D. M., Brazier, R., Parsons, A., Wainwright, J., Nichols, M., 2007. Sediment transfer and
908 storage in dryland headwater streams. Geomorphology 88, 152-166.
909 Reaney, S. M., Bracken, L. J., & Kirkby, M. J., 2014. The importance of surface controls on overland
910 flow connectivity in semi-arid environments: results from a numerical experimental
911 approach. Hydrological Processes, 28, 2116-2128.
912 Reid, I., Laronne, J. B., Powell, D. M., 1995. The Nahal Yatir bedload database: Sediment dynamics in
913 a gravel-bed ephemeral stream. Earth Surface Processes and Landforms 20, 845-857.
914 Riesco Martin, J., Mora García, M., de Pablo Davila, F., Rivas Soriano, L., 2014. Regimes of intense
915 precipitation in the Spanish Mediterranean area. Atmos. Res. 137, 66–79.

916 Schick, A., Lekach, J., 1987. A high magnitude flood in the Sinai desert. In: Mayer, L., Nash, D. (Eds.)
917 Catastrophic Flooding. Allen and Unwin, Boston, pp 381-410.
918 Schick, A., Lekach, J., 1993. An evaluation of two ten-year sediment budgets, Nahal Yael, Israel.
919 Physical Geography 14, 225-238.
920 Schumm, S.A., 1973. Geomorphic thresholds and complex response of drainage systems. In:
921 Morisawa, M. (Ed.), Fluvial Geomorphology. University of New York, Binghamton, pp. 301–
922 310
923 Schumm, S.A., 1979. Geomorphic thresholds: the concept and its applications. Transactions of the
924 Institute of British Geographers New Series 4, 485–515.
925 Smith, M.W., Carrivick, J.L., Hooke, J., Kirkby, M.J., 2014. Reconstructing Flash Flood Magnitudes
926 Using 'Structure-from-Motion': a rapid assessment tool. Journal of Hydrology 519, 1914-
927 1927.
928 Thompson, C., Croke, J., 2013. Geomorphic effects, flood power, and channel competence of a
929 catastrophic flood in confined and unconfined reaches of the upper Lockyer valley, southeast
930 Queensland, Australia. Geomorphology 197, 156-169.
931 Thompson, C., Croke, J., Grove, J., Khanal, G., 2013. Spatio-temporal changes in river bank mass
932 failures in the Lockyer Valley, Queensland, Australia. Geomorphology 191, 129-141.
933 Trigg, M. A., Michaelides, K., Neal, J. C., & Bates, P. D., 2013. Surface water connectivity dynamics of
934 a large scale extreme flood. Journal of Hydrology, 505, 138-149.
935 Wainwright, J., 1996. Hillslope response to extreme storm events: The example of the Vaison-La-
936 Romaine event. In: Anderson, M G and Brooks, S M. (Eds.) Advances in Hillslope Processes,
937 vol 2. John Wiley and Sons; Chichester, pp 997-1026..
938 Werritty, A., Leys, K. F., 2001. The sensitivity of Scottish rivers and upland valley floors to recent
939 environmental change. Catena 42, 251-273.
940 Wolman, M.G., Gerson, R., 1978. Relative scales of time and effectiveness of climate in watershed
941 geomorphology. Earth Surface Processes 3, 189–208.

942 Wolman, M.G., Miller, J.P., 1960. Magnitude and frequency of forces in geomorphic
943 processes. Journal of Geology 68, 54–74.
944 Wong, J. S., Freer, J. E., Bates, P. D., Sear, D. A., Stephens E. M., 2015. Sensitivity of a hydraulic model
945 to channel erosion uncertainty during extreme flooding. Hydrological Processes 29, 261-
946 279.

947

948 Figure captions

949 Fig. 1. Map of location of study reaches in Guadalentín basin, southeast Spain.

950 Fig. 2. Photographs of study reaches before and after 2012 flood event: (A) Nogalte sites, (B)
951 Torrealvilla sites.

952 Fig. 3. (A) Hydrograph of 28 September 2012 flow event on Nogalte as measured at CHS gauge at
953 Puerto Lumbreras. (B) Peak discharges in the Nogalte channel calculated from surveyed cross
954 sections; CHS is gauged discharge at Puerto Lumbreras; Leeds points are data surveyed by Kirkby and
955 Smith (Leeds University).

956 Fig. 4 Site map, cross sections, long profile, and post-flood DEM at site Nog 1.

957 Fig. 5. Site map, cross sections, long profile, and post-flood DEM at site Nog 2.

958 Fig. 6. Site map, cross sections, long profile, and post-flood DEM at site Nog Mon.

959 Fig. 7. Site map, cross sections, long profile, and post-flood DEM at site Torrealvilla Oliva.

960 Fig. 8. Site map, cross sections, long profile, and post-flood DEM at site Torrealvilla Aqueduct.

961 Fig. 9. Site map, cross sections, long profile, and post-flood DEM at site Torrealvilla Pintor.

962 Fig. 10. Difference of pre- and post-flood DEMs (DoDs) for: Nogalte sites (A) Nog 1, (B) Nog 2, (C) Nog
963 Mon, and Torrealvilla sites (D) Oliva, (E) Aqueduct, (F) Pintor

964 Fig. 11. Magnitude of bankfull channel capacity change in relation to peak flow hydraulic values at
965 surveyed cross sections.

966 Fig. 12. Net change in cross-sectional area in relation to peak flow hydraulics at sites.

967 Fig. 13. Maximum erosion and maximum deposition measured at cross sections in relation to peak
968 flow hydraulics.

969 Fig. 14. Morphological changes in relation to channel morphology: (A) change in cross-sectional
970 capacity, (B) gross area change.

971 Fig. 15. Peak discharge in relation to catchment area for the three Nogalte sites, plotted on
972 Thompson and Croke (2013) graph of major flood events and with Costa's (1987) envelope curve.

973

974

975 Table 1

976 Characteristics of measured channel reaches, SE Spain

977

| Catchment | Site | Lithology | Catchment area ($km^2$) | Distance downstream (km) | Channel and valley morphology | Gradient | Floodplain width (m) | Bankfull channel width (m) | Bankfull channel depth (m) | Vegetation | |
|---|---|---|---|---|---|---|---|---|---|---|---|
| | | | | | | | | | | Channel | Floodplain |
| Nogalte | 1 | Schist | 6.9 | 6.5 | Shallow channel | 0.0161 | 20 | 1.4-10.3 | 0.21-0.79 | Sparse | Retama |
| | 2 | Schist | 39.1 | 11.5 | Braided, unconfined | 0.0199 | 70 | 9.5-15.3 | 0.30-0.84 | Shrubs | Retama |
| | Mon | Schist | 102.7 | 18.5 | Braided, unconfined | 0.0188 | 120 | 12.7-24.6 | 0.34-1.15 | Retama | Agriculture |
| Torrealvilla | Oliva | Marl & Gravel | 73.2 | 16.0 | Single channel, moderate wide valley | 0.0099 | 25 | 2.2-5.2 | 0.24-0.74 | Bare | Tamarisk/ agriculture |
| | Aqueduct | Marl & Gravel | 54.4 | 7.0 | Single, confined | 0.0072 | 25 | 2.6-8.1 | 0.40-1.55 | Bare | Shrubs, Tamarisk |
| | Pintor | Marl & Gravel | 253.8 | 25.0 | Single, embanked | 0.0074 | 35 | 8.7-18.8 | 0.31-0.73 | Bare | Tamarisk/ fields |

978 Table 2

979 Hydraulic values calculated at cross sections for a) post-flood morphology, and b) pre-flood morphology

| Site | XS | Flood level Elevation m | Flood level Crest recorder m | W m | Dav m | Slope | Manning n | Velocity m $s^{-1}$ | Discharge $m^3$ $s^{-1}$ | Post-flood Q site $m^3$ $s^{-1}$ | Shear stress N $m^{-2}$ | Power W $m^{-3}$ | Unit power W $m^{-2}$ | Froude number |
|---|---|---|---|---|---|---|---|---|---|---|---|---|---|---|
| **(a) POST- FLOOD MORPHOLOGY** | | | | | | | | | | | | | | |
| **Nog1** | **X3** | 840.4 | | 22.1 | 0.65 | 0.0246 | 0.04 | 2.57 | 36.84 | | 129 | 8875 | 402 | 1.02 |
| | **XCR** | 839.55 | 1.2 | 24.31 | 0.70 | 0.0183 | 0.04 | 2.28 | 38.70 | 38 | 100 | 6925 | 285 | 0.87 |
| | **X10** | 839.05 | | 27.42 | 0.57 | 0.0460 | 0.04 | 3.56 | 55.94 | | 245 | 25207 | 919 | 1.50 |
| **Nog 2** | **X1** | 744 | | 85.5 | 1.15 | 0.0146 | 0.04 | 3.28 | 321.61 | | 162 | 45928 | 537 | 0.98 |
| | **X2** | 743.55 | | 82 | 1.67 | 0.0214 | 0.05 | 4.00 | 546.58 | 550 | 335 | 114682 | 1399 | 0.99 |
| | **X3** | 743.04 | | 80.19 | 1.70 | 0.0196 | 0.05 | 3.94 | 537.40 | | 316 | 103224 | 1287 | 0.97 |
| | **XCR** | 741.63 | 2.13 | 79.4 | 1.48 | 0.0214 | 0.05 | 4.00 | 546.58 | | 335 | 114682 | 1444 | 1.05 |
| **NogMon** | **X1** | 601.6 | | 129.07 | 1.63 | 0.0230 | 0.054 | 3.87 | 816.02 | 1050 | 364 | 183932 | 1425 | 0.97 |
| | **X2** | 600.6 | 2.58 | 133.22 | 1.31 | 0.0258 | 0.04 | 4.70 | 822.64 | | 320 | 208237 | 1563 | 1.31 |

| | | | | | | | | | | | | | | |
|---|---|---|---|---|---|---|---|---|---|---|---|---|---|---|
| **Oliva** | **X2** | 502.68 | | 43.45 | 0.95 | 0.01200 | 0.04 | 2.61 | 107.35 | 110 | 109.56 | 12624 | 290.55 | 0.86 |
| | **X3** | 502.64 | | 31.99 | 1.80 | 0.01196 | 0.04 | 3.15 | 148.17 | | 115.35 | 17366 | 542.87 | 0.75 |
| | **X5** | 501.66 | | 37.72 | 0.86 | 0.01196 | 0.04 | 2.39 | 77.46 | | 95.66 | 9078 | 240.68 | 0.82 |
| | **X6** | 501.7 | | 32.71 | 1.05 | 0.03800 | 0.06 | 3.20 | 109.53 | | 354.41 | 40790 | 1247.02 | 1.00 |
| | **XCR** | 500.89 | 2.29 | 23 | 1.28 | 0.02750 | 0.04 | 4.01 | 117.94 | | 253.98 | 31785 | 1381.95 | 1.13 |
| **Aqued** | **XCRN** | 438.45 | 3.06 | 26.53 | 2.43 | 0.01243 | 0.04 | 4.76 | 306.79 | 260 | 270.98 | 37371 | 1408.62 | 0.98 |
| | **X10** | 438.28 | | 32.13 | 2.20 | 0.00536 | 0.04 | 3.32 | 234.87 | | 105.22 | 12337 | 383.98 | 0.72 |
| | **TA3** | 437.84 | | 26.93 | 1.94 | 0.01130 | 0.04 | 3.76 | 196.08 | | 374.30 | 21713 | 806.29 | 0.86 |
| | **X20** | 437.71 | | 28.18 | 2.41 | 0.00536 | 0.04 | 3.11 | 210.93 | | 115.89 | 11080 | 393.18 | 0.64 |
| **Pintor** | **X1** | 433.19 | | 43.2 | 2.50 | 0.01103 | 0.04 | 3.83 | 345.52 | 420.00 | 189.66 | 37342 | 983 | 0.77 |
| | **XCR** | 432.95 | 3.45 | 51.83 | 1.90 | 0.01182 | 0.04 | 3.99 | 392.80 | | 205.66 | 45500 | 877.87 | 0.93 |
| | **X2** | 432.9 9 | | 55.28 | 2.16 | 0.01179 | 0.04 | 4.17 | 450.96 | | 237.73 | 52096 | 942.40 | 0.91 |

980

981

**(b) PRE- FLOOD MORPHOLOGY**

| | | | | | | | | | | | | | | |
|---|---|---|---|---|---|---|---|---|---|---|---|---|---|---|
| **Nog1** | **X3** | 840.4 | | 22.1 | 0.80 | 0.0246 | 0.04 | 3.34 | 58.71 | | 189 | 14143 | 640 | 0.92 |
| | **XCR** | 839.55 | 1.2 | 24.31 | 0.74 | 0.0183 | 0.04 | 2.41 | 43.02 | 38 | 108 | 7699 | 317 | 0.85 |
| | **X10** | 839.05 | | 27.42 | 0.51 | 0.0460 | 0.04 | 3.33 | 46.17 | | 221 | 20805 | 759 | 1.60 |
| **Nog 2** | **X1** | 744 | | 85.5 | 1.28 | 0.0146 | 0.04 | 3.58 | 392.68 | | 184 | 56077 | 656 | 0.92 |
| | **X2** | 743.55 | | 82 | 1.89 | 0.0214 | 0.04 | 5.02 | 777.63 | 550 | 337 | 163161 | 1990 | 0.93 |
| | **X3** | 743.04 | | 76.89 | 1.80 | 0.0196 | 0.04 | 5.14 | 710.23 | | 341 | 136422 | 1774 | 0.94 |
| | **XCR** | 741.63 | 2.13 | 79.4 | 1.39 | 0.0214 | 0.04 | 5.26 | 579.52 | | 361 | 121593 | 1531 | 1.09 |
| **NogMon** | **X1** | 601.6 | | 126.12 | 1.25 | 0.0230 | 0.04 | 6.02 | 1496.75 | 1050 | 449 | 337367 | 2675 | 1.11 |
| | **X2** | 600.6 | 2.8 | 133.22 | 1.60 | 0.0258 | 0.04 | 5.59 | 1193.81 | | 414 | 302193 | 2268 | 1.19 |
| **Oliva** | **X2** | 502.68 | | 42.33 | 0.83 | 0.01200 | 0.04 | 2.38 | 83.67 | 110 | 109.58 | 9840 | 232 | 0.83 |
| | **X3** | 502.64 | | 31.99 | 1.78 | 0.01196 | 0.04 | 2.69 | 152.93 | | 144.97 | 17925 | 560 | 0.64 |
| | **X5** | 501.66 | | 37.72 | 0.84 | 0.01196 | 0.04 | 2.37 | 75.05 | | 95.66 | 8796 | 233 | 0.83 |
| | **X6** | 501.7 | | 32.71 | 1.08 | 0.03800 | 0.06 | 3.24 | 114.85 | | 354.41 | 42770 | 1308 | 1.00 |
| | **XCR** | 500.89 | 2.29 | 23 | 1.26 | 0.02750 | 0.04 | 3.94 | 113.87 | | 256.58 | 30688 | 1334 | 1.12 |

| | | | | | | | | | | | | | | |
|---|---|---|---|---|---|---|---|---|---|---|---|---|---|---|
| **Aqued** | **XCRN** | 438.45 | 3.06 | 26.53 | 2.25 | 0.01243 | 0.04 | 4.53 | 270.16 | 260 | 270.97 | 32909 | 1240 | 0.97 |
| | **X10** | 438.28 | | 32.13 | 2.22 | 0.00536 | 0.04 | 2.98 | 212.44 | | 128.04 | 11159 | 347 | 0.64 |
| | **TA3** | 437.84 | | 27.81 | 1.90 | 0.01130 | 0.04 | 3.75 | 198.43 | | 185.77 | 21975 | 790 | 0.87 |
| | **X20** | 437.71 | | 28.18 | 2.33 | 0.00536 | 0.04 | 3.06 | 200.80 | | 115.87 | 10547 | 374 | 0.64 |
| **Pintor** | **X1** | 433.19 | | 43 | 2.50 | 0.01103 | 0.04 | 3.83 | 341.11 | 420 | 189.66 | 36865 | 970 | 0.77 |
| | **XCR** | 432.95 | 3.45 | 51.83 | 1.88 | 0.01182 | 0.04 | 3.98 | 388.72 | | 205.77 | 45027 | 869 | 0.93 |
| | **X2** | 432.99 | | 55.28 | 2.16 | 0.01179 | 0.04 | 4.17 | 451.67 | | 218.89 | 52178 | 944 | 0.91 |

984 Table 3

985 Depths of erosion and deposition and changes in cross-sectional area at each site (CR = crest recorder flood stage. ch = channel, fp =floodplain)

986

| | | Flood elevn | CR stage | Bank-full elevn | Erosion | | | Deposition | | | Maximum | | CS Area | | | |
|---|---|---|---|---|---|---|---|---|---|---|---|---|---|---|---|---|
| | | m | m | m | m | | | m | | | m | | $m^2$ | | | |
| **Site** | **XS** | | | | **ch** | **bar** | **fp** | **ch** | **bar** | **fp** | **Max erosn** | **Max depn** | **Net change** | **Gross change** | **Erosn** | **Depn** |
| **Nog1** | **X3** | 840.4 | | 839.89 | 0 | 0 | 0 | 0.23 | 0.42 | 0 | 0 | 0.42 | 3.27 | 3.27 | 0 | 3.27 |
| | **XCR** | 839.55 | 1.2 | 838.60 | 0.38 | 0.25 | 0 | 0 | 0.14 | 0.29 | -0.38 | 0.29 | 0.8 | 2.4 | -0.8 | 1.6 |
| | **X10** | 839.05 | | 838.7 | 0.64 | 0.15 | 0 | 0.1 | 0 | 0 | -0.64 | 0.1 | -2.1 | 2.4 | -2.3 | 0.2 |
| **Nog 2** | **X1** | 744 | | 743 | 0 | 0.61 | 0 | 0.2 | 0.85 | 0.05 | -0.61 | 0.85 | 13.9 | 26.1 | -6.1 | 20 |
| | **X2** | 743.55 | | 742.5 | 0.85 | 0 | 0 | 0.17 | 0.81 | 0.21 | -0.85 | 0.81 | 5.8 | 32.8 | -13.5 | 19.3 |
| | **X3** | 743.04 | | 741.76 | 0.72 | 0.55 | 0 | 0.24 | 0.61 | 0 | -0.72 | 0.61 | 2.7 | 30.5 | -13.9 | 16.6 |
| | **XCR** | 741.63 | 2.13 | 740.44 | 0.83 | 0 | 0.34 | 0 | 0.79 | 0.18 | -0.83 | 0.79 | 7 | 30.2 | -11.6 | 18.6 |
| **NogMon** | **X1** | 601.6 | | 600.14 | 0.46 | 0.2 | 0 | 0.38 | 0.81 | 0 | -0.46 | 0.81 | 46.3 | 51.5 | -2.6 | 48.9 |
| | **X2** | 600.6 | 2.58 | 599.71 | 0.29 | 0 | 0 | 0.32 | 0.91 | 0.24 | -0.29 | 0.91 | 44 | 62.2 | -9.1 | 53.1 |

| | | | | | | | | | | | | | | | | |
|---|---|---|---|---|---|---|---|---|---|---|---|---|---|---|---|---|
| **Oliva** | **X2** | 502.68 | | 501.5 | -0.34 | 0 | 0 | 0 | 0 | 0 | -0.34 | 0 | -0.82 | 0.82 | -0.82 | 0 |
| | **X3** | 502.64 | | 501.0 | -0.33 | 0 | 0 | 0 | 0 | 0.01 | -0.33 | 0.01 | -0.65 | 0.75 | -0.7 | 0.05 |
| | **X5** | 501.66 | | 500.9 | -0.36 | 0 | 0 | 0 | 0 | 0.1 | -0.36 | 0.1 | -0.82 | 2.5 | -1.66 | 0.84 |
| | **X6** | 501.7 | | 500.7 | 0.37 | 0 | 0 | 0.04 | 0 | 0.12 | -0.37 | 0.12 | -2.03 | 3.03 | -2.53 | 0.5 |
| | **XCR** | 500.89 | 2.29 | 499.6 | -0.56 | 0 | 0 | 0 | 0 | 0.16 | -0.56 | 0.16 | -0.6 | 2.6 | -1.6 | 1 |
| **Aqued** | **XCRN** | 438.45 | 3.06 | 435.8 | 0 | -0.63 | -1.03 | 0 | 0 | 0.4 | -1.03 | 0.4 | -4.83 | 7.23 | -6.03 | 1.20 |
| | **X10** | 438.28 | | 435.9 | 0.62 | 0.45 | 0 | 0 | 0.18 | 0.41 | -0.62 | 0.41 | 0.7 | 5.90 | -2.6 | 3.30 |
| | **TA3** | 437.84 | | 435.7 | 0.4 | 0.33 | 0 | 0 | 0 | 0.57 | -0.4 | 0.57 | 1 | 8 | -3.5 | 4.50 |
| | **X20** | 437.71 | | 435.5 | 0.08 | 0.33 | 0.47 | 0.23 | 0 | 0.33 | -0.47 | 0.33 | (-2.5) | (6.7) | | |
| **Pintor** | **X1** | 433.19 | | 431.0 | 0.4 | 0.18 | - | 0 | 0.08 | - | -0.4 | 0.08 | -1.2 | 1.8 | -1.5 | 0.3 |
| | **XCR** | 432.95 | 3.45 | 430.0 | 0.26 | 0.19 | 0.31 | 0.14 | 0 | 0.17 | -0.31 | 0.17 | -0.7 | 0.9 | -0.8 | 0.1 |
| | **X2** | 432.99 | | 430.4 | 0.12 | 0 | 0 | 0.15 | 0.04 | 0.22 | -0.12 | 0.22 | 0.4 | 0.6 | -0.1 | 0.5 |

(Human impacts)

990 Table 4

991 Particle sizes of post-flood deposits; quadrat max and quadrat regular are measurements from digital photographs of 0.5 m quadrats of largest 10 particles
992 and at 25 regular grid points, respectively

| | | | Quadrat max | Quadrat regular | | Bulk samples - weight | | | |
|---|---|---|---|---|---|---|---|---|---|
| Channel | Sample | | Avge 10 mm | Avge mm | St devn mm | d50 mm | d84 mm | %>2 mm | %silt-clay |
| **Nog1** | **VQ1** | **Bar** | 47.5 | 13.1 | 23.4 | | | | |
| | **2** | **Channel** | 34 | 12.6 | 21.7 | | | | |
| | **3** | **Floodplain** | 29.8 | 5.1 | 12.8 | | | | |
| | **4** | **Bar** | 19 | 4.4 | 4.4 | | | | |
| | **5** | **Channel** | 16.7 | 3.8 | 2.2 | | | | |
| | **SS1** | **Channel** | 26.8 | 7.8 | 5.3 | 7 | 30 | 74% | 10.8% |
| | **SS2** | **Channel** | 20.8 | 4.4 | 2.1 | 2.8 | 9 | 59% | 5% |
| **Nog2** | **1** | **Channel** | 29.4 | 6.4 | 7.8 | | | | |
| | **2** | **Bar** | 42.7 | 7.5 | 9.9 | | | | |
| | **3** | **Bar** | 38.5 | 11.7 | 19.8 | | | | |
| | **SS1** | **Channel** | 14.1 | 4.2 | 3.2 | 1.9 | 7 | 47% | 7.6% |
| | **SS2** | **Bar** | 23.3 | 5 | 3.7 | 3.5 | 7 | 64% | 5% |
| **NogMon** | **1** | **Low bar** | 35.1 | 13.4 | 23.2 | | | | |
| | **2** | **Channel** | 40.8 | 12.4 | 22.2 | | | | |
| | **3** | **Bar** | 26.2 | 2.4 | 2.7 | | | | |
| | **4** | **Bar** | 18.3 | 6 | 5.7 | | | | |
| | **SS1** | **Channel** | 23.2 | 4 | 3.3 | 2.4 | 7 | 56% | 6% |
| | **SS2** | **Low bar** | 31.3 | 9.2 | 9.2 | 6 | 23 | 69% | 12.8% |
| | **SS3** | **High bar** | 17.7 | 4.9 | 4.4 | 1.8 | 6 | 43% | 6.1% |
| **Oliva** | **1** | **Floodpain** | 27.3 | | | | | | |
| | **2** | **Channel** | 37.2 | | | | | | |
| | **3** | **Floodpain** | 25.5 | | | | | | |
| | **4** | **Floodpain** | <2 | | | | | | |
| | **SS1** | **Channel** | | | | 5 | 16.2 | 73% | 0% |
| | **SS2** | **Floodpain** | | | | 0.062 | 0.13 | 0% | 51% |
| **Aqued** | **1** | **Floodpain** | 13.7 | | | | | | |

| | | | | | | | | |
|---|---|---|---|---|---|---|---|---|
| | | **2** | **Bar** | 3.5 | | | | |
| | | **4** | **Channel** | 48.8 | | | | |
| | | **5** | **Floodpain** | 22.3 | | | | |
| | **SS1** | | **Bar** | | 2.9 | 11 | 58% | 4% |
| | **SS2** | | **Floodpain** | | 0.51 | 1.1 | 6% | 23% |
| | | | | | | | | |
| **Pintor** | | **1** | **Channel** | 48.3 | | | | |
| | | **2** | **Channel** | 68.5 | | | | |
| | | **3** | **Channel** | 89.2 | | | | |
| | | **4** | **Bar** | 54.5 | | | | |

993

994

995 Table 5

996 Correlation coefficients of relations between variables for Nogalte and Torrealvilla sites; shaded cells indicate significant values at $p$ = 0.05 level

| | Change | | | | | | | | | |
|---|---|---|---|---|---|---|---|---|---|---|
| | **Area *Flood level*** | **Area *Bankfull*** | **Depth *Flood level*** | **Depth *Bankfull*** | **Max erosion** | **Max deposi-tion** | **Net change** | **Gross change** | **Gross erosion** | **Gross deposition** |
| | $m^2$ | $m^2$ | m | m | m | m | $m^2$ | $m^2$ | $m^2$ | $m^2$ |
| | | | | | **Nogalte** | | | | | |
| **Discharge ($m^3$ $s^{-1}$)** | -0.71 | -0.83 | 0.14 | -0.53 | -0.26 | 0.84 | 0.78 | 0.98 | -0.58 | 0.93 |
| **Power (W $m^{-1}$)** | 0.40 | -0.90 | 0.00 | -0.46 | -0.14 | 0.75 | 0.83 | 0.97 | -0.50 | 0.94 |
| **Velocity (m $s^{-1}$)** | 0.00 | -0.69 | -0.10 | -0.73 | -0.45 | 0.63 | 0.54 | 0.83 | -0.71 | 0.73 |
| **Unit power (W $m^{-2}$)** | -0.46 | -0.75 | 0.14 | 0.22 | -0.48 | 0.59 | 0.52 | 0.81 | -0.69 | 0.71 |
| **Shear stress (N $m^{-2}$)** | -0.48 | -0.89 | 0.24 | -0.47 | -0.51 | 0.55 | 0.51 | 0.77 | -0.64 | 0.69 |
| **Width (m)** | -0.79 | -0.88 | 0.10 | -0.46 | -0.20 | 0.87 | 0.86 | 0.99 | -0.47 | 0.97 |
| **Depth av (m)** | -0.39 | -0.83 | -0.32 | -0.77 | -0.47 | 0.81 | 0.32 | 0.73 | -0.89 | 0.56 |
| **Area ($m^2$)** | -0.82 | -0.89 | 0.17 | -0.45 | -0.20 | 0.83 | 0.84 | 0.97 | -0.47 | 0.95 |
| **W/D** | -0.75 | -0.83 | 0.45 | -0.37 | 0.00 | 0.57 | 0.89 | 0.79 | 0.00 | 0.88 |

## Torrealvilla

| | | | | | | | | | | |
|---|---|---|---|---|---|---|---|---|---|---|
| **Discharge ($m^3 s^{-1}$)** | 0.10 | -0.14 | 0.14 | -0.32 | -0.26 | 0.28 | 0.00 | 0.00 | 0.00 | -0.10 |
| **Power ($W m^{-1}$)** | -0.28 | -0.40 | -0.17 | -0.39 | 0.10 | 0.00 | -0.30 | 0.00 | 0.00 | -0.32 |
| **Velocity ($m s^{-1}$)** | 0.00 | -0.20 | 0.24 | -0.20 | -0.41 | 0.44 | -0.35 | 0.48 | -0.36 | 0.10 |
| **Unit power ($W m^{-2}$)** | -0.17 | -0.36 | 0.10 | 0.00 | -0.36 | 0.14 | -0.53 | 0.28 | -0.42 | -0.10 |
| **Shear stress ($N m^{-2}$)** | -0.40 | 0.17 | 0.39 | 0.40 | -0.10 | 0.41 | -0.20 | 0.51 | -0.10 | 0.35 |
| **Width (m)** | 0.00 | 0.40 | -0.33 | -0.28 | 0.53 | -0.39 | -0.20 | -0.52 | 0.46 | -0.47 |
| **Depth av (m)** | 0.00 | -0.14 | 0.17 | -0.20 | -0.24 | 0.50 | 0.00 | 0.17 | -0.17 | 0.26 |
| **Area ($m^2$)** | -0.17 | -0.17 | -0.14 | -0.35 | 0.28 | 0.14 | 0.20 | -0.22 | 0.20 | -0.10 |
| **W/D** | 0.24 | 0.00 | -0.22 | 0.00 | 0.46 | -0.62 | 0.00 | -0.39 | 0.28 | -0.46 |

997

998

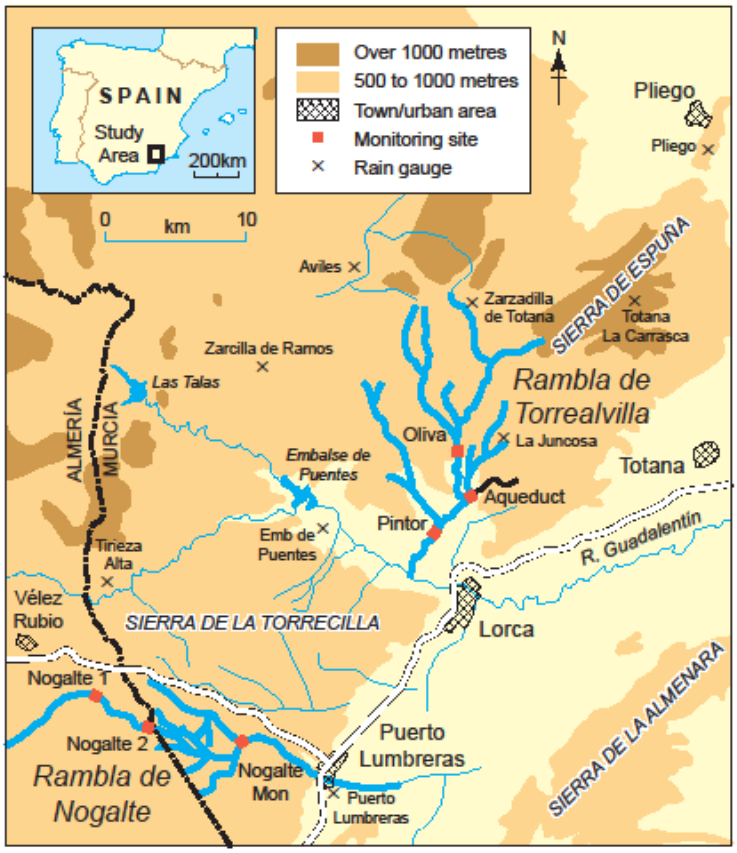
SPAIN
Study Area
200km
Over 1000 metres
500 to 1000 metres
Town/urban area
Monitoring site
Rain gauge
N
0 km 10
Pliego
Pliego
Aviles
Zarzadilla de Totana
SIERRA DE ESPUÑA
Totana
La Carrasca
Zarcilla de Ramos
Las Talas
Rambla de Torrealvilla
ALMERÍA
MURCIA
Oliva
La Juncosa
Totana
Embalse de Puentes
Aqueduct
Pintor
Emb de Puentes
R. Guadalentín
Tiñeza Alta
Vélez Rubio
SIERRA DE LA TORRECILLA
Lorca
Nogalte 1
Nogalte 2
Rambla de Nogalte
Nogalte Mon
Puerto Lumbreras
Puerto Lumbreras
SIERRA DE LA ALMENARA

999 Fig.1

(A) Nogalte


1000

Fig. 2a

(B) Torrealvilla


1001

Fig.2b

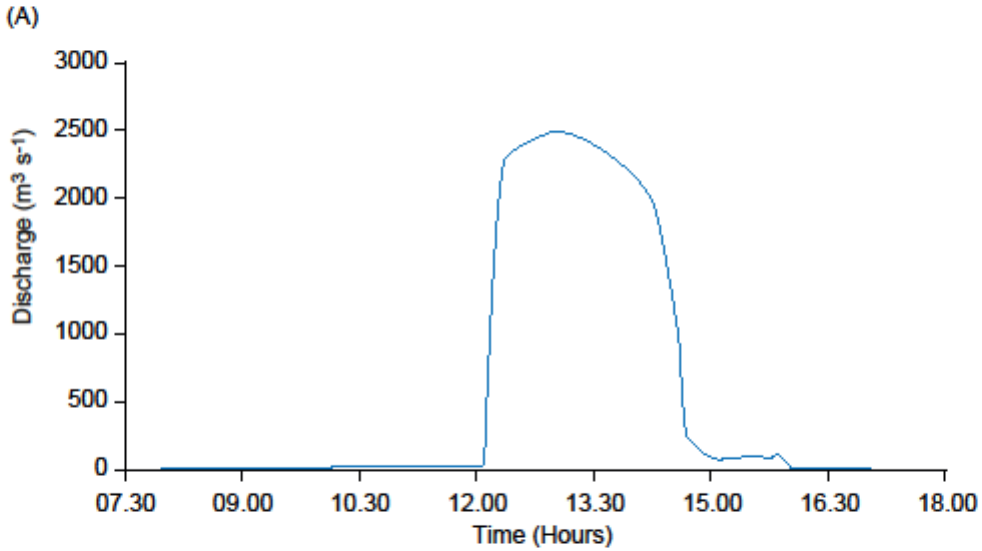
(A)
3000
2500
2000
1500
1000
500
0
Discharge (m³ s⁻¹)
07.30
09.00
10.30
12.00
13.30
15.00
16.30
18.00
Time (Hours)

1002 Fig. 3a

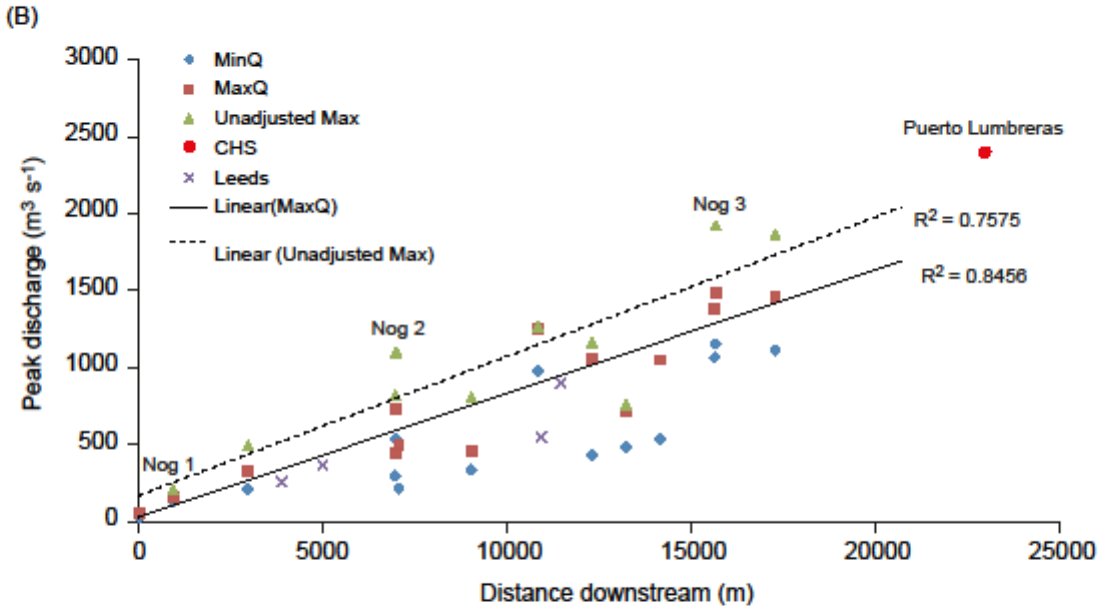
(B)
MinQ
MaxQ
Unadjusted Max
CHS
Leeds
Linear(MaxQ)
Linear (Unadjusted Max)
Puerto Lumbreras
Nog 3
Nog 2
Nog 1
R2 = 0.7575
R2 = 0.8456
Peak discharge (m3 s-1)
Distance downstream (m)
0
500
1000
1500
2000
2500
3000
0
5000
10000
15000
20000
25000

1003

Fig 3b

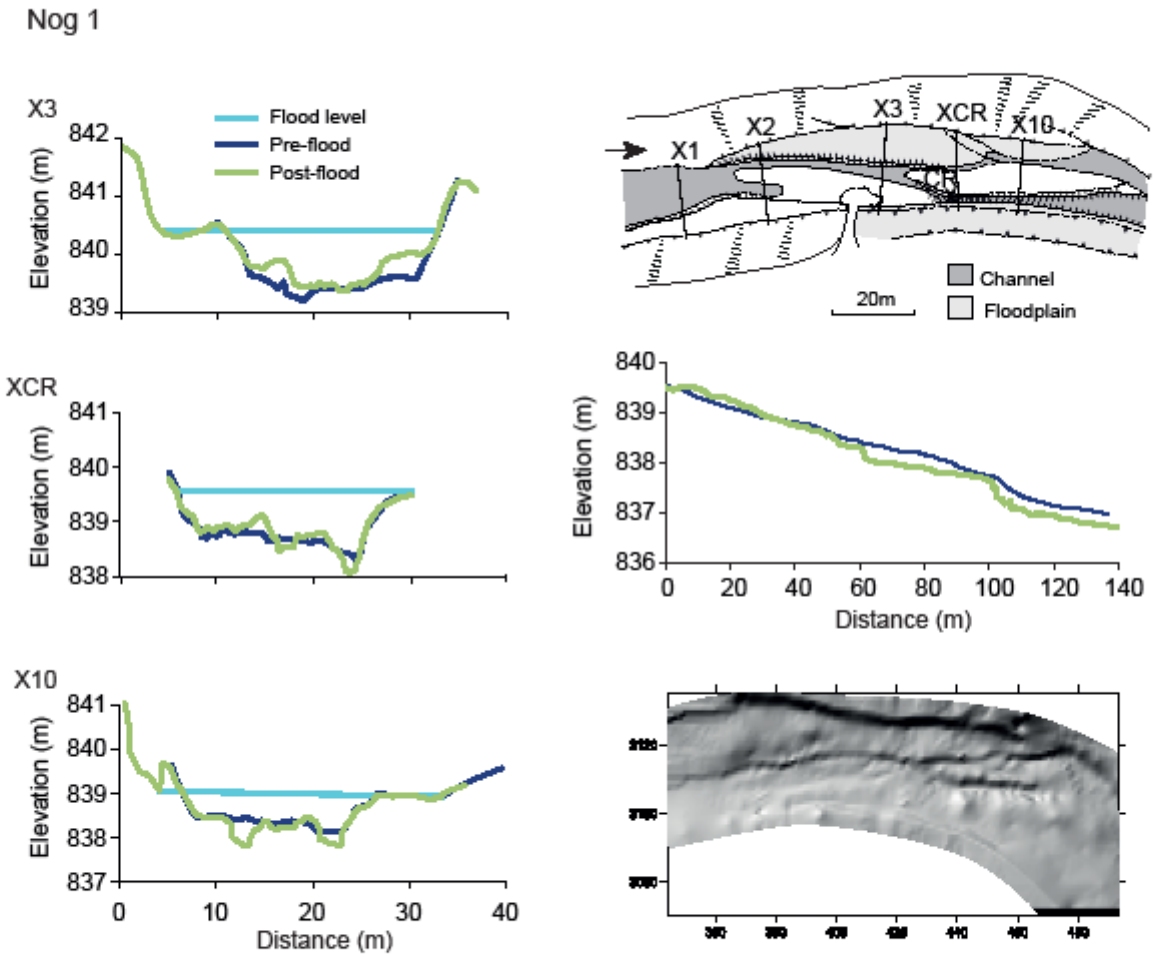
Nog 1
X3
Flood level
Pre-flood
Post-flood
Elevation (m)
842
841
840
839
X1
X2
X3
XCR
X10
CR
Channel
Floodplain
20m
XCR
841
840
839
838
840
839
838
837
836
0
20
40
60
80
100
120
140
Distance (m)
X10
841
840
839
838
837
0
10
20
30
40
Distance (m)

1004

Fig. 4

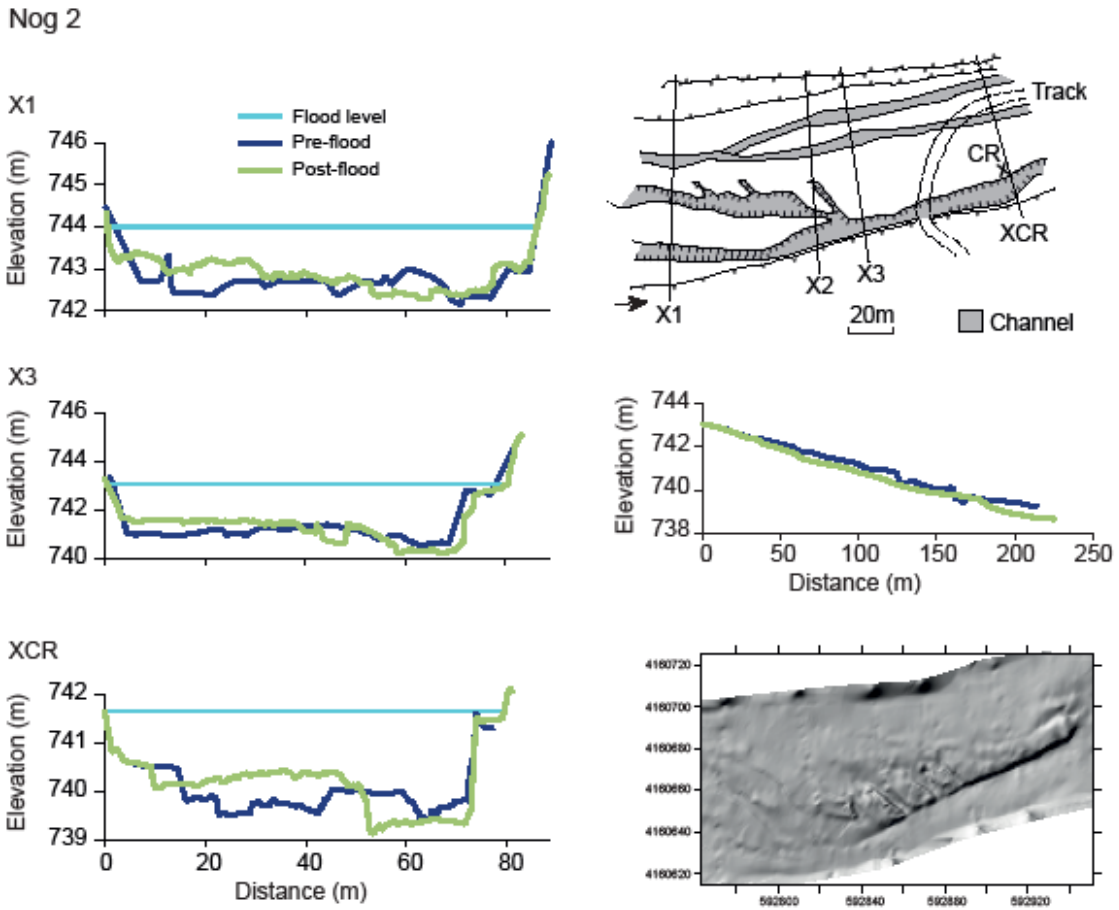
Nog 2
X1
Flood level
Pre-flood
Post-flood
Elevation (m)
746
745
744
743
742
Track
CR
XCR
X2
X3
X1
20m
Channel
X3
Elevation (m)
746
744
742
740
744
742
740
738
0
50
100
150
200
250
Distance (m)
XCR
Elevation (m)
742
741
740
739
0
20
40
60
80
Distance (m)
4160720
4160700
4160680
4160660
4160640
4160620
592800
592840
592880
592920

1005

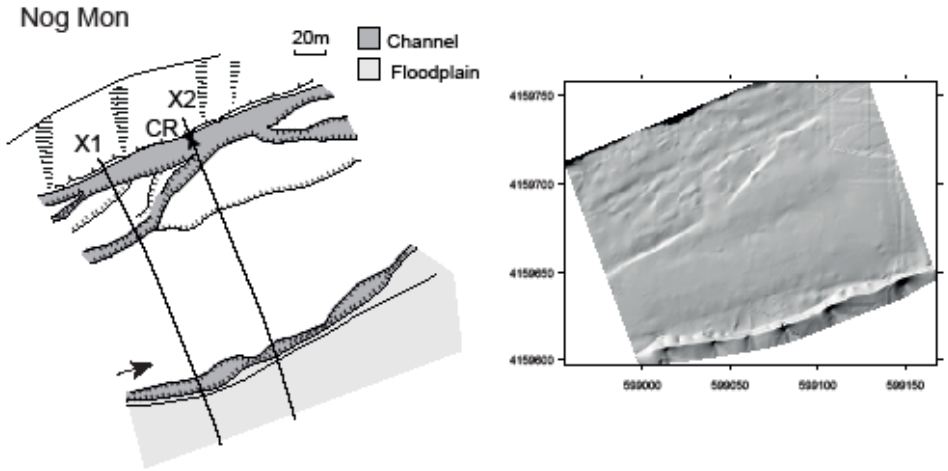
Nog Mon
20m
Channel
Floodplain
X1
X2
CR1
4159750
4159700
4159650
4159600
599000
599050
599100
599150

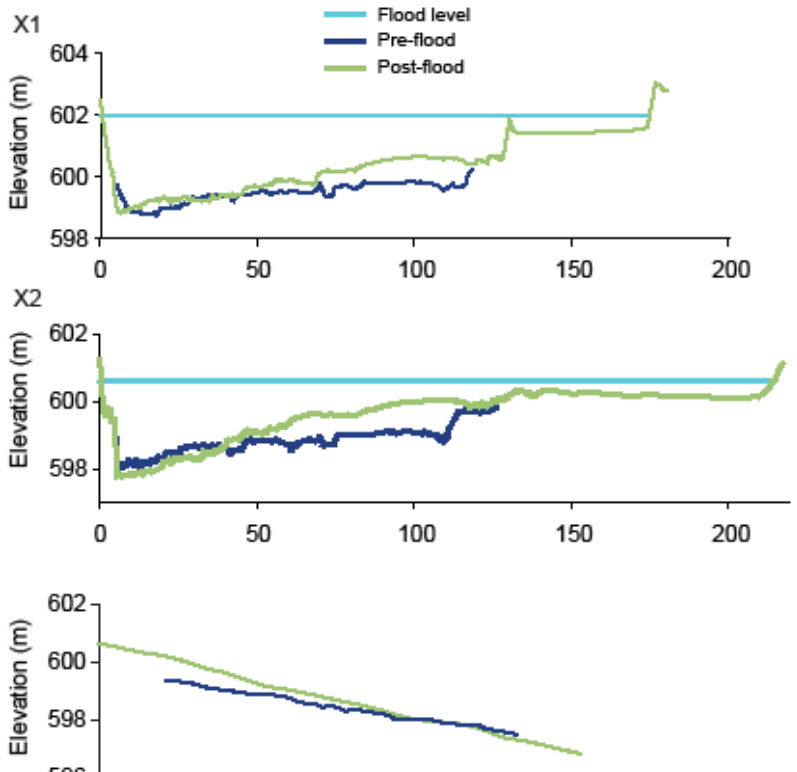
X1
Flood level
Pre-flood
Post-flood
Elevation (m)
604
602
600
598
0
50
100
150
200
X2
Elevation (m)
602
600
598
0
50
100
150
200
Elevation (m)
602
600
598

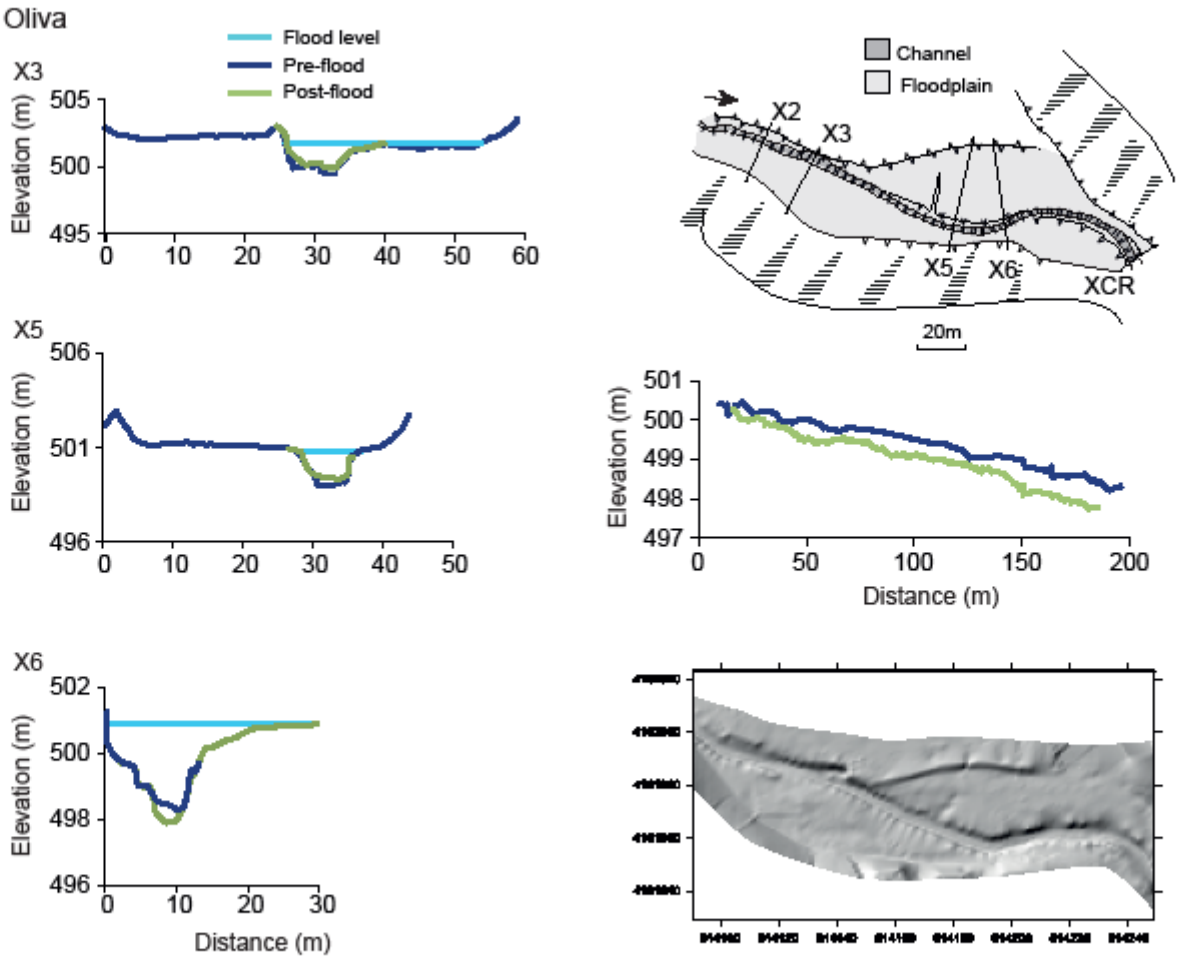
Oliva
Flood level
Pre-flood
Post-flood
X3
Elevation (m)
505
500
495
0
10
20
30
40
50
60
X5
506
501
496
0
10
20
30
40
50
X6
502
500
498
496
0
10
20
30
Distance (m)
Channel
Floodplain
X2
X3
X5
X6
XCR
20m
501
500
499
498
497
0
50
100
150
200
Distance (m)

1007

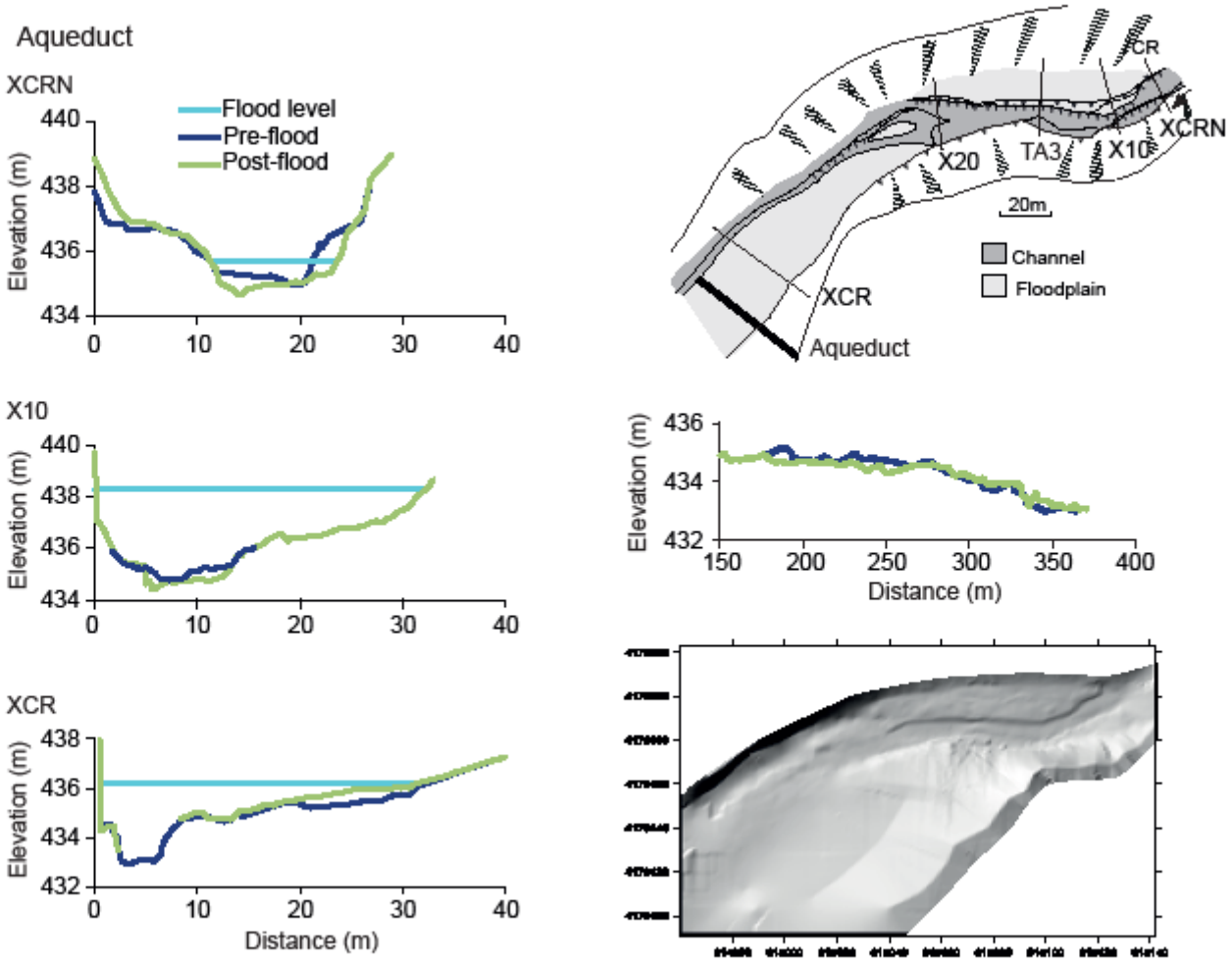
Aqueduct
XCRN
Flood level
Pre-flood
Post-flood
Elevation (m)
440
438
436
434
0
10
20
30
40
X10
Elevation (m)
440
438
436
434
0
10
20
30
40
XCR
Elevation (m)
438
436
434
432
0
10
20
30
40
Distance (m)
CR
XCRN
X20
TA3
X10
20m
Channel
Floodplain
XCR
Aqueduct
Elevation (m)
436
434
432
150
200
250
300
350
400
Distance (m)

1008

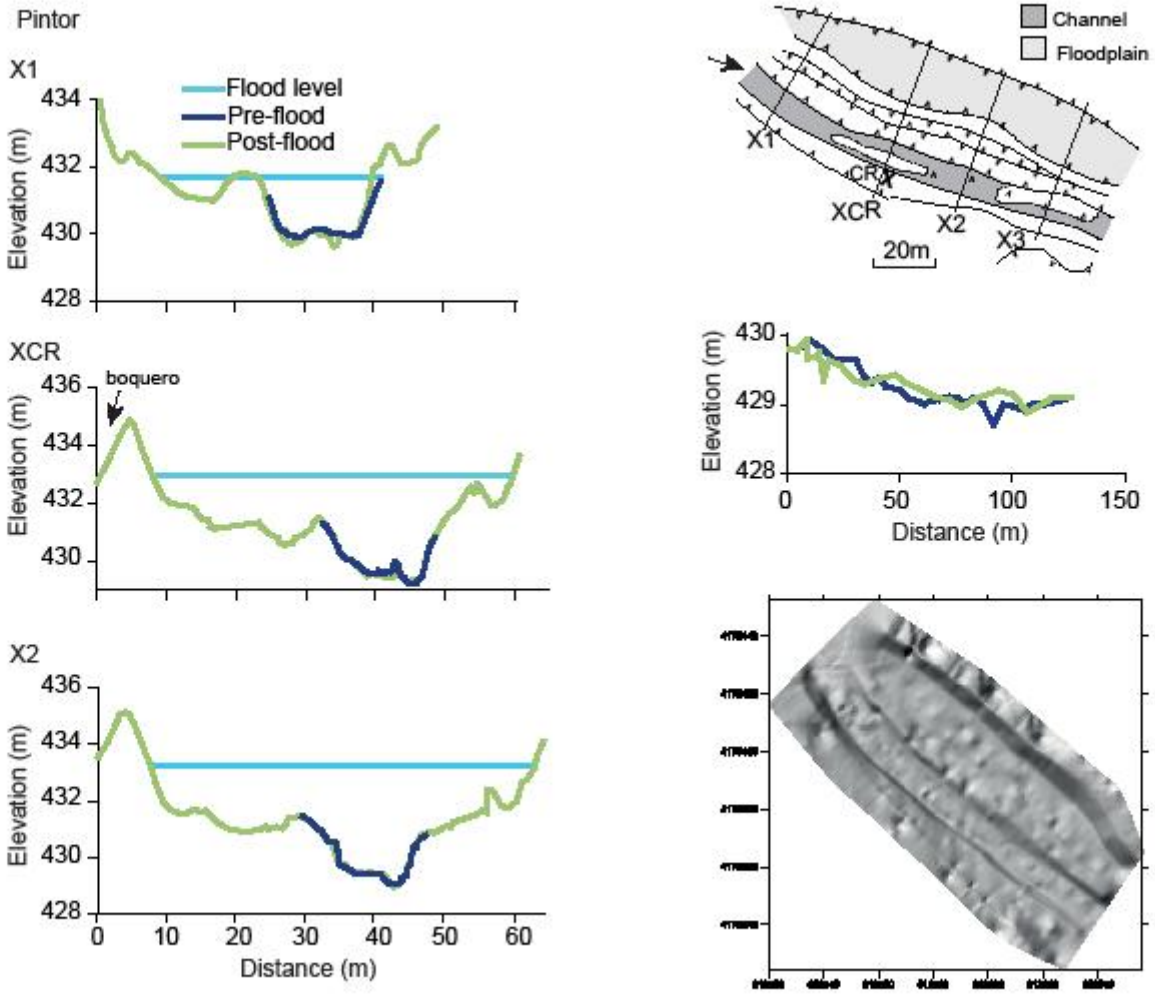
Pintor
X1
Flood level
Pre-flood
Post-flood
Elevation (m)
434
432
430
428
XCR
boquero
436
434
432
430
X2
436
434
432
430
428
0
10
20
30
40
50
60
Distance (m)
Channel
Floodplain
X1
CR
XCR
X2
X3
20m
Elevation (m)
430
429
428
0
50
100
150
Distance (m)

1009

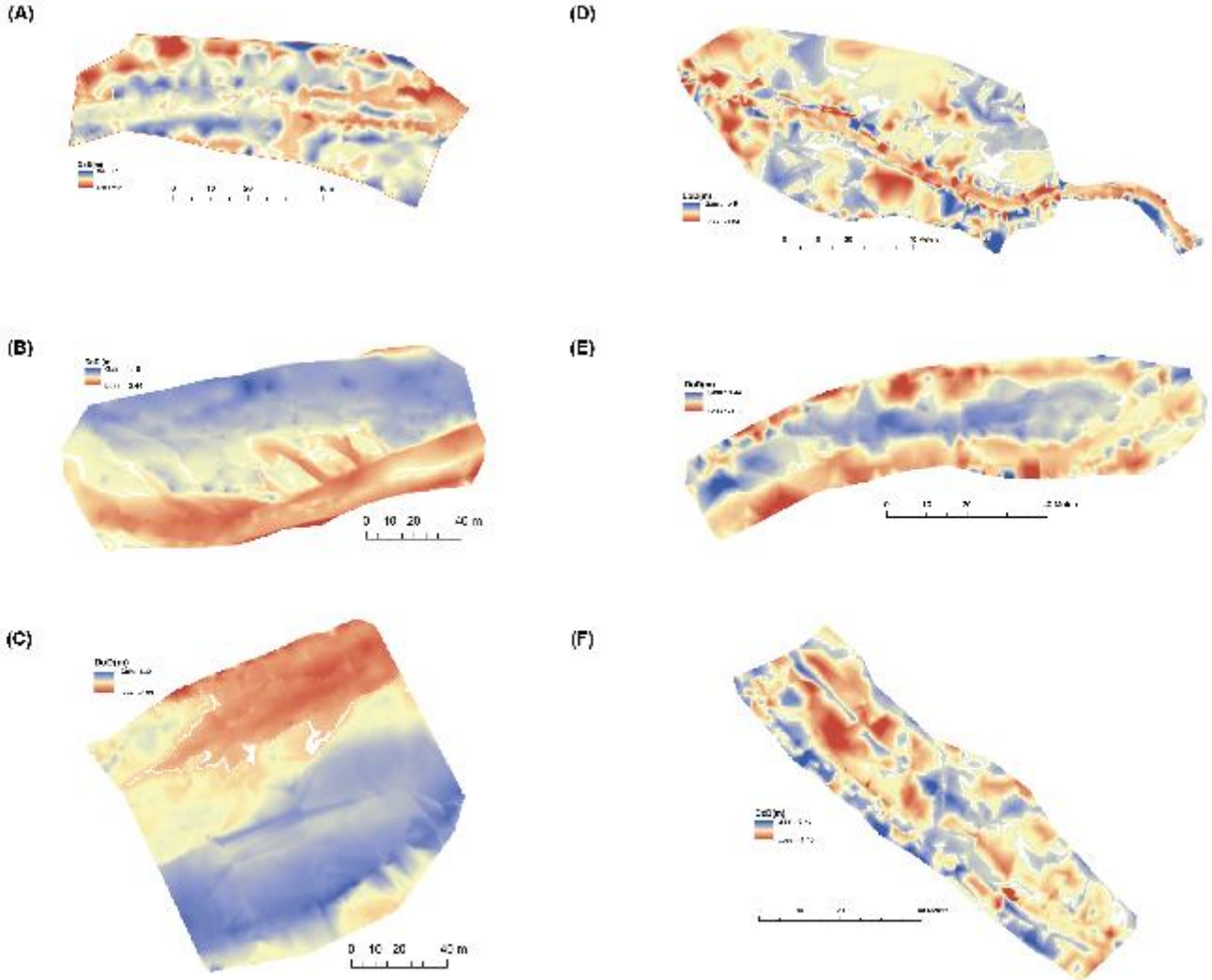


1010

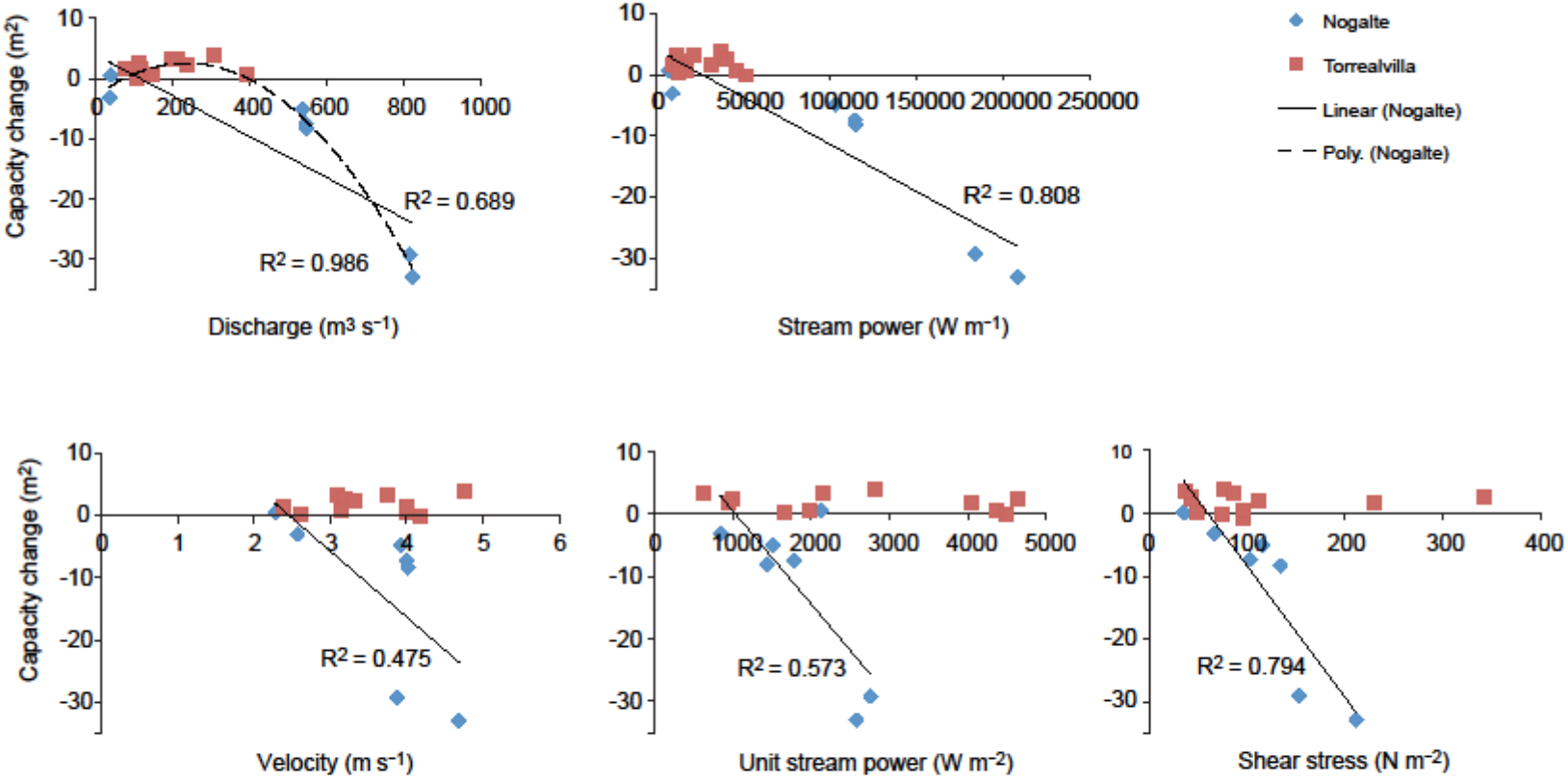
Capacity change (m²)
Discharge (m³ s⁻¹)
R² = 0.689
R² = 0.986
Stream power (W m⁻¹)
R² = 0.808
Velocity (m s⁻¹)
R² = 0.475
Unit stream power (W m⁻²)
R² = 0.573
Shear stress (N m⁻²)
R² = 0.794
Nogalte
Torrealvilla
Linear (Nogalte)
Poly. (Nogalte)

1011

Fig. 11

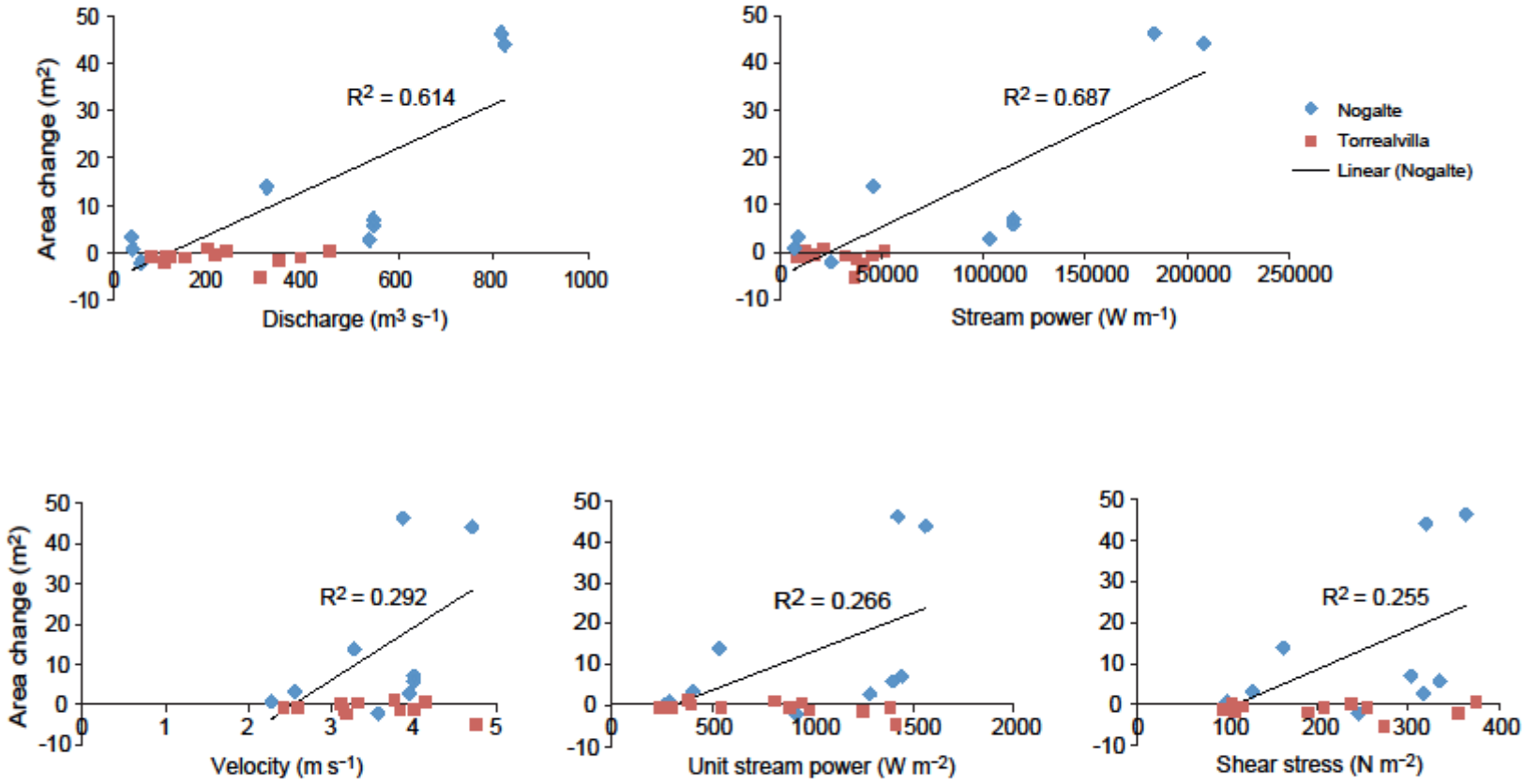
Area change (m²)
Discharge (m³ s⁻¹)
R² = 0.614
Stream power (W m⁻¹)
R² = 0.687
Nogalte
Torrealvilla
Linear (Nogalte)
Velocity (m s⁻¹)
R² = 0.292
Unit stream power (W m⁻²)
R² = 0.266
Shear stress (N m⁻²)
R² = 0.255

1012

Fig. 12

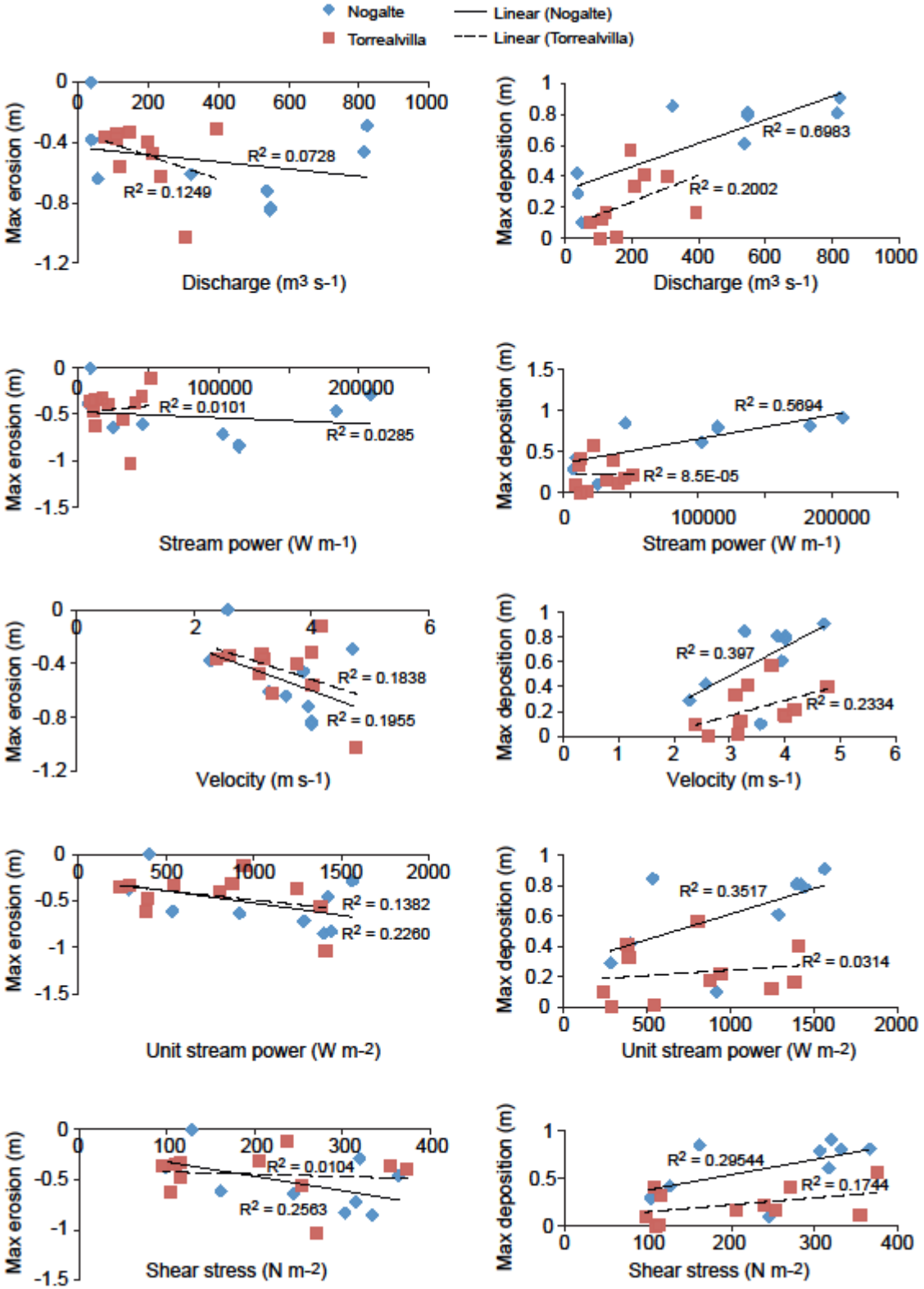
Nogalte
Torrealvilla
Linear (Nogalte)
Linear (Torrealvilla)
Max erosion (m)
Discharge (m3 s-1)
R2 = 0.0728
R2 = 0.1249
Max deposition (m)
R2 = 0.6983
R2 = 0.2002
Stream power (W m-1)
R2 = 0.0101
R2 = 0.0285
R2 = 0.5694
R2 = 8.5E-05
Velocity (m s-1)
R2 = 0.1838
R2 = 0.1955
R2 = 0.397
R2 = 0.2334
Unit stream power (W m-2)
R2 = 0.1382
R2 = 0.2260
R2 = 0.3517
R2 = 0.0314
Shear stress (N m-2)
R2 = 0.0104
R2 = 0.2563
R2 = 0.29544
R2 = 0.1744

1013

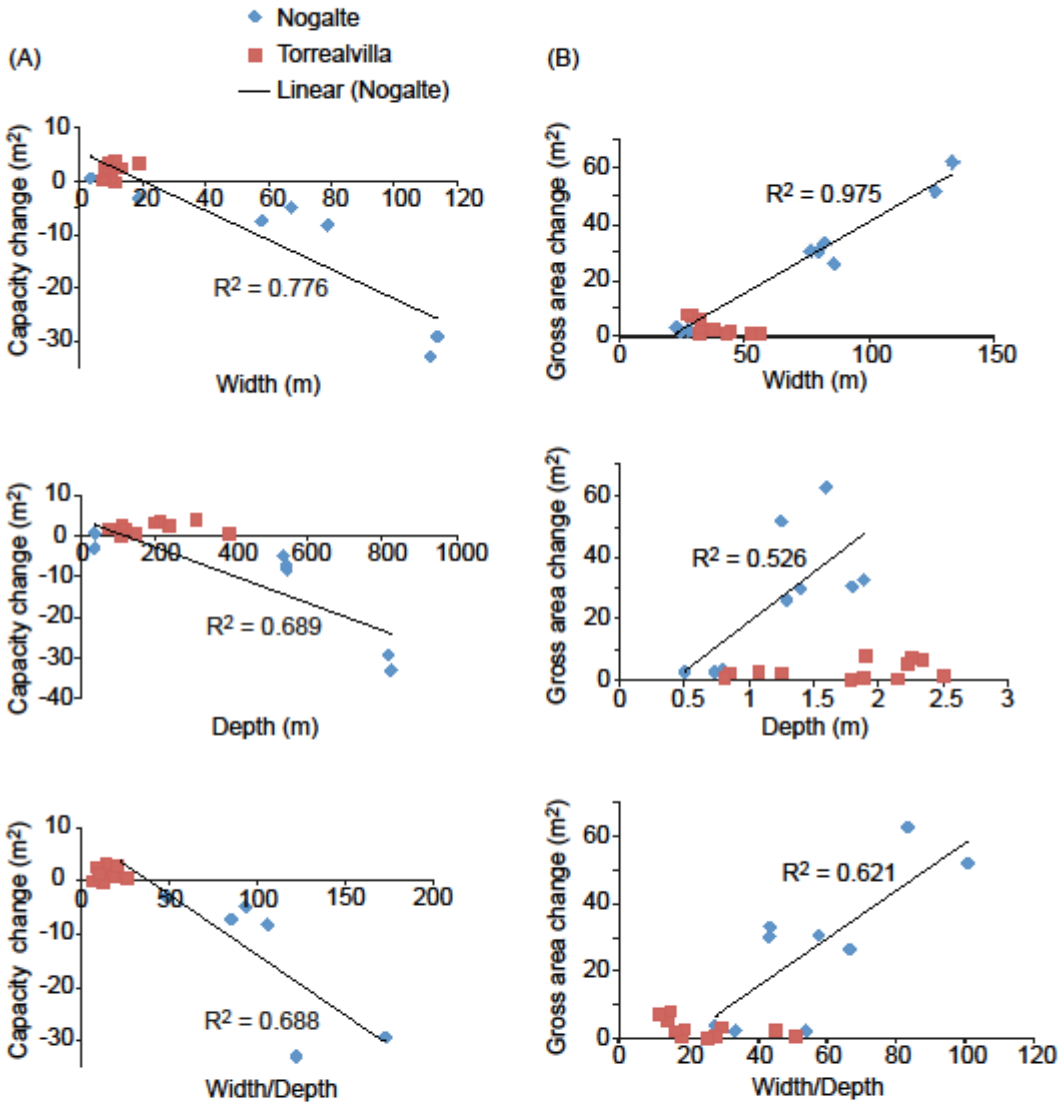


1014
1015 Fig. 14

1016

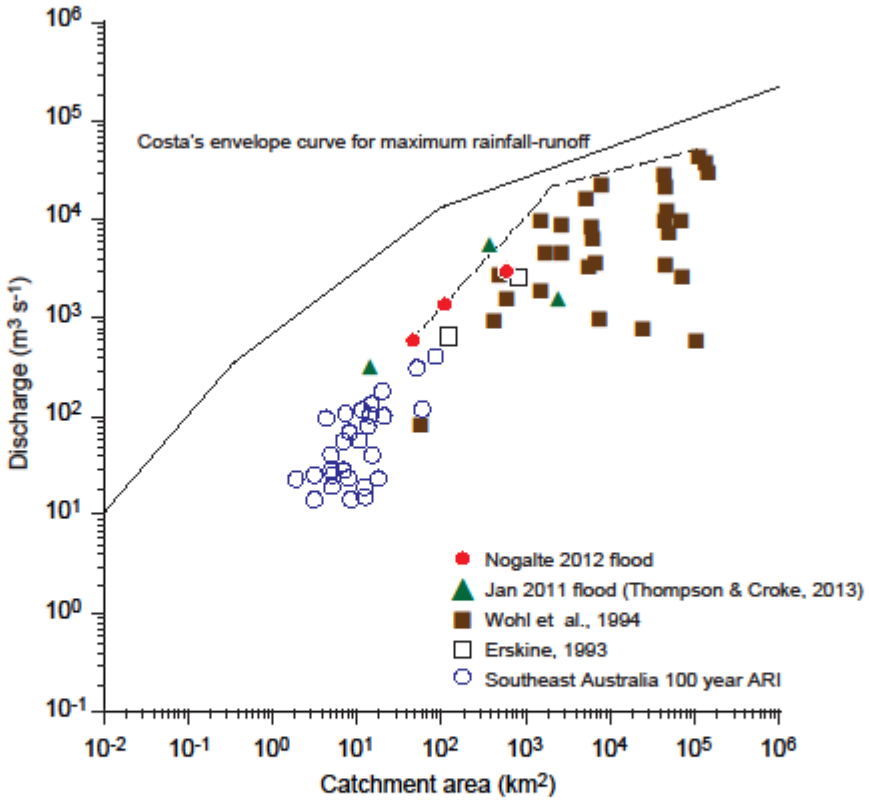


1017
1018 Fig. 15

1019